بِسْمِ ٱللَّهِ ٱلرَّحْمَٰنِ ٱلرَّحِيمِ

Sudan University of Science &Technology

College of Graduate Studies
Biomedical Engineering
Department

MRI Phase Mismapping Image Artifact correction

تصحيح التشوهات الناتجه عن فقدان الطور في صور الرنين المغنطيسي

A Thesis Submitted in partial Fulfillment of the Requirements for the M.Sc. degree in Biomedical Engineering

Presented By:

Ashraf Abrahim Abdallah ahmed

Supervised By:

Dr. Mawia Ahmed Hassan

JUNE 2016

ACKNOWLEDGEMENT

Praise be to Allah, Lord of Universe.

My deepest gratitude are due to all who have contributed to this humble work, without their assistance the task would be impossible.

In particular I would like to acknowledge a deep gratitude to my supervisor Dr. Mawia Ahmed Hassan for his non ending assistance and patience. I am also grateful to him for helping me with his unlimited experience and orientation for further knowledge and publication and good would communication.

I express my appreciation of the support of Dr. Omer E. H. Hamid always supporting me and push me towards the knowledge and development.

Special thanks are extended to all the staff of the Department of medical engineering for their understanding and support.

Grateful thanks are due to all who helped me in the tedious work of analysis, printing and arrangement of this text.

Last but not least, a very special thanks for my big family father and mother they are every time pushing my dreams towards, and I would like to acknowledge the assistance of my wife sulima, she is the real MSc maker by supporting and offering the chance for reading and researching and special thanks to my kids smiles.

TABLE OF CONTENTS

LIST OF FIGURES

LIST OF TABLES

ABSTRACT

MRI machine one of the most significant diagnostic modalities. The only restriction that affects the MRI image is that imaging procedure take very long time comparing with CT scan and other diagnostic modalities, thus old patient, children and the illness people cannot stay without movement inside the magnet therefore artifact will affect the MRI image and several miss analysis may occur especially in the neuroanatomical measurements. Many procedure has been use to solve this problem for example before during and after the MRI image reconstruction. in this study the effectiveness of a new retrospective motion correction technique has been applied and tested. Three different section MRI image (coronal, sagittal and axial) were used and given different correction results. That was by develop algorithm to correct the motion blur in the MRI image that corrupted by patient rigid motion. Wiener filter was used as the main restoration procedure by means of angle and length estimation of the motion blur. Motion blur angle and length were estimated using Hough transformer. The technique was applied and tested several time, it gave acceptable correction result in the sagittal image compare with the coronal one but the technique was result in the least motion blur correction in the axial image. Signal to noise ratio was calculated for every image to figure out the degree of the correction technique according to the different estimated angle and length. Signal to noise ratio values were to be through with correction result.

المستخلص

يعتبر الرنين المغنطيسي من اهم الاجهزه التشخيصيه غير ان عيبه الوحيد يكمن في طول فتره الفحص مقارنه بجهاز الاشعه المقطعيه وبعض الاجهزه الاخري ونجد ان غالبيه المرضي من كبار السن والاطفال والمرضي في اوضاعهم الحرجه لايطيقون المكوث لفتره طويله داخل المغنطيس . مما يؤثر سلبا علي جوده الصوره وبالتالي تحليلهاوتشخيصها تشخيصا خاطا . تمت العديد من الحاولات لتصحيح التشوهات الناتجه من حركه المريض داخل المغنطيس منها طرق تستخدم قبل تكوين الصوره وبعضها اثناء تكوين الصوره والاخر يقوم بتصحيح التشوات في الصوره بعد تكوينها.

في الدراسه التاليه تم تطبيق طريقه جديده لتصحيح التشوهات في صوره الرنين الناتجه من حركه المريض اثناء التصوير داخل المغنطيس وذلك بعد تكوين الصوره . تم اختيار ثلاث صور رنين مغنطيسي لمقاطع مختلفه في الراس لمريض تحرك اثناء التصوير. تم استخدام مرشح الونر في الماتلاب كمرشح اساسي لعمليه تصحيح التشوهات بالاضافه لمرشحات اخري . تم الحصول علي نتائج ممتازه في مقطعين (الجانبي والامامي)ونتائج متوسطه في حاله المقطع الاخير العرضي

CHAPTER ONE

1. INTRODUCTION

1.1 General overview

Magnetic resonance imaging (MRI) is an imaging technique used primarily in medical settings to produce high quality images of the inside of the human body. MRI is based on the principles of nuclear magnetic resonance (NMR), a spectroscopic technique used by scientists to obtain microscopic chemical and physical information about molecules .The technique was called magnetic resonance imaging rather than nuclear magnetic resonance imaging (NMRI) because of the negative connotations associated with the word nuclear. [1]

MRI scanning is always kept at a high standard quality by taking firm unshaken pictures of appointed body areas of patients. This brings up the problem of patient motion which interferes with the accuracy and precision of the scanning process, leading to improper analysis and misinterpretation of findings, thus misguiding important decisions based on MRI scan results. Also, running an MRI demands high operating expenses to be approved, taking into consideration the electrical supply to the scan, maintenance costs and valued time consumption. Therefore, it is mandatory to detect patient motion which is one of the main causes of MRI artifact. From this point, the idea of this project was born, to create algorithm that detects patient motion values (length and angle of the blur motion) and determines the direction and level of the motion. This would help to reduce cost and time, and help in achieving a higher quality image.

1.2 The Problem Statement

Artifacts caused by head and body motion pose a significant problem for the in vivo magnetic resonance imaging (MRI) of the human brain. Motion artifacts adversely affect the ability to accurately characterize the size, shape, and tissue properties of brain structures in both research subjects and clinical patients. In cognitive neuroscience applications, cross-sectional and longitudinal effects in neuroanatomical measurements are relatively small, making them easily obscured by distortions arising from patient and subject movement. Image quality is often degraded by motion artifacts, including image blurring and ghosting [1]. A number of techniques are employed to help in get rid of these problems: one is to prevent the motion occurring using sedation or physical restraints. Sedation involves risk [2] and also adds complication to the scan. Physically restraining patients is only partially effective.

1.3 Thesis Objectives

The objectives of this Thesis are:

1. The main objective at this work is to develop algorithm to correct the motion blur in the MRI image that corrupted by patient rigid motion. depend on the estimated angle and length of the blur

2. Develop an algorithm which can be estimate the angle and the length of motion blur MRI image.

3- Determine the suitable angle and length which result in the maximum correction.

1.4 Thesis Organization

This Thesis consist of six chapters, first chapter is an introduction, second chapter will provide the theoretical background, third chapter which introduce the previous studies and the literature reviews, forth chapter will describe the research methodology, the result obtained and discussion of these results given in the fifth chapter and in the last chapter will contain conclusion and recommendations future work should be considered.

CHAPTER TWO
2. THEORETICAL BACKGROUN

2.1 Introduction:

This chapter describes the working principle of MRI, applications of MRI techniques, as well as hardware of MRI. Several artifacts related to MRI are also discussed in this chapter plus the K-space" data acquisition and image reconstruction.

The description of MRI image motion classification according to two different approach are shown as well as the proposed MRI image motion correction. Finally wiener filter and Hough transform also describe in this chapter.

2.2 The working principle of MRI:

Clinical Magnetic Resonance Imaging (MRI) uses the magnetic properties of hydrogen and its interaction with both a large external magnetic field and radio waves to produce highly detailed images of the human body. Firstly, some basic principles of magnetism, the magnetic properties of the hydrogen nucleus, and its interaction with the externally applied magnetic field were explained. In its early days, MRI was known as NMR. This stands for Nuclear Magnetic Resonance. Although the name has changed (primarily due to the negative connotation of the word "nuclear"), the basic principles are the same. The images are obtained from the magnetic resonance properties of nuclear particles (specifically hydrogen). In order to perform MRI, a strong magnetic field is needed. The field strength of the

magnets used for MR is measured in units of Tesla. One Tesla is equal to 10,000 Gauss. The magnetic field of the earth is approximately 0.5 Gauss. Given that relationship, a 1.0 T magnet has a magnetic field approximately 20,000 times stronger than that of the earth. The type of magnets used for MR imaging usually belongs to one of three types; permanent, resistive, and superconductive. A permanent magnet is sometimes referred to as a vertical field magnet. These magnets are constructed of two magnets (one at each pole). The patient lies on a scanning table between these two plates. Advantages of these systems are: Relatively low cost, No electricity or cryogenic liquids are needed to maintain the magnetic field, their more open design may help alleviate some patient anxiety, nearly nonexistent fringe field. It should be noted that not all vertical field magnets are permanent magnets. Resistive magnets are constructed from a coil of wire. The more turns to the coil, and the more current in the coil, the higher the magnetic field. These types of magnets are most often designed to produce a horizontal field due to their solenoid design the nucleus of the hydrogen atom contains a single proton. Because of this, as previously mentioned, it possesses a significant magnetic moment. The proton will behave as a tiny bar magnet as shown in fig (2.1)

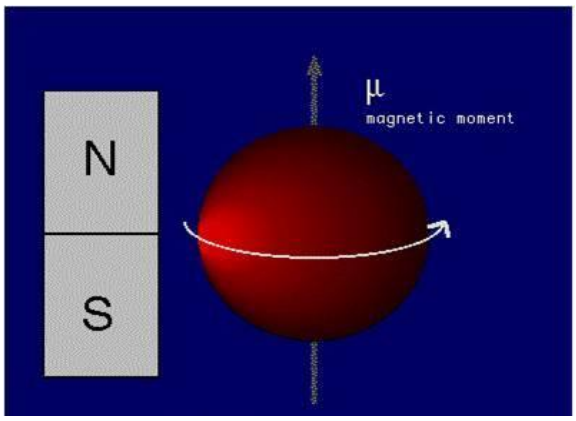

Figure 2.1 principle of MRI. [3]

Because of the spin characteristics of the proton, if it is placed in a large external magnetic field, it will assume one of two possible positions. It will align (at a slight angle) in either a parallel or anti-parallel with the direction of the magnetic field. [3]

- 2.3 Applications of MRI Techniques:

MRI is used as a diagnostic tool for identification of medical conditions and for monitoring their treatment courses, such as:

- Tumors of the chest, abdomen or pelvis.
- Coronary artery disease and heart problems including the aorta, coronary arteries and blood vessels, by examining the size and thickness of the chambers of the heart and the extent of damage caused by a heart attack or progressive heart disease.
- Tumors and other abnormalities of the reproductive organs (e.g., uterus, ovaries, testicles, prostate).
- Causes of pelvic pain in women, such as endometriosis.[3]

2.4 Hardware of MRI:

The basic components of an NMR imaging system [4] as shown in fig (2.2)

- Magnets.
- Radio-frequency coils.
- Gradients.
- Shimming
- Computer

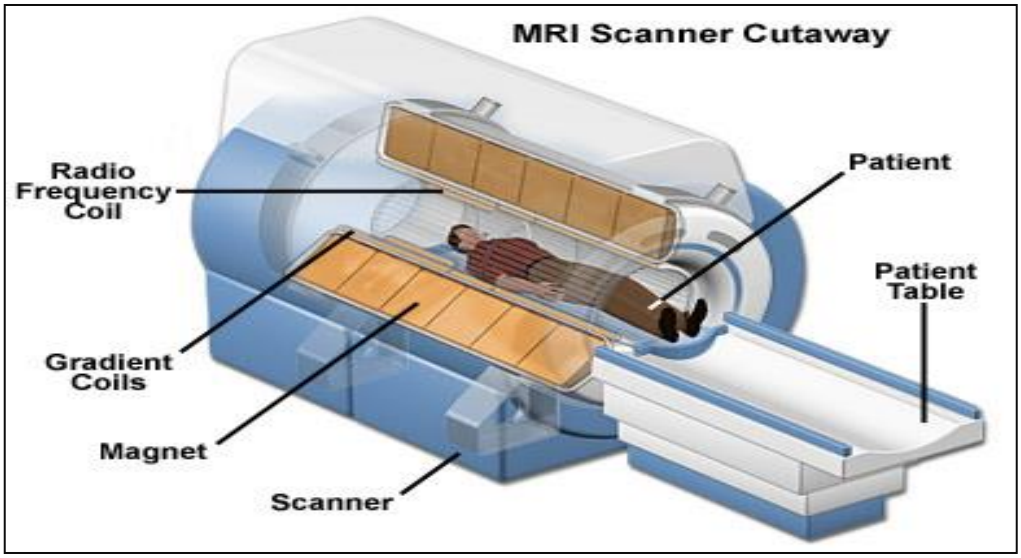

Figure 2.2 Hardware components of MRI. [5]

2.4.1 Magnets of MRI:

There are three several different types of magnets that can be used to produce the magnetic field [6]

- Permanent magnets.
- Resistive magnets.
- Superconducting magnets.

2.4.1.1 Permanent magnets:

A permanent magnet consists of a material, which has been magnetized such that it won't lose its magnetic field, (like the ones you put on your refrigerator). The field strength is usually very low and ranges between 0.064T ~ 0.3T. Permanent magnets have usually an open design, which is more comfortable for the patient. [7]

2.4.1.2 Resistive magnets:

Resistive magnets are very large electro magnets. The magnetic field is generated by a current, which runs through loops of wire. Resistive magnets come in two flavors: air-core and iron-core. The field strength can be up to 0.3 Tesla. They produce a lot of heat, which requires water-cooling. They need a lot of power to run, and are usually switched off when not in use to conserve power [7]

2.4.1.3 Superconducting magnets:

Today's most commonly used magnets are superconducting magnets. The magnetic field is generated by a current, which runs through a loop of wire. The wire is surrounded with a coolant, such as liquid helium, to reduce the electric resistance of the wire. Once a system is energized, it won't lose its magnetic field. Superconductivity allows for systems with very high field strengths up to 12 Tesla. The ones that are most used in clinical environments run at 1.5 Tesla. Most superconducting magnets are bore type magnets. [7]

2.4.2 Radio-frequency coils:

RF coils are needed to transmit and receive radio-frequency waves used in MRI scanners. RF coils are one of the most important components that affect image quality. Current MRI scanners have a range of RF coils suitable to acquire images of all body parts. There are two types of RF coils, volume coils and surface coils. [7]

2.4.3 Gradients coils:

Gradient coils provide a linear gradation or slope of the magnetic field strength from one end of the magnet to the other. This is achieved by passing current through the gradient coils .The direction of the current through the coil determines whether the magnetic field strength is increased or decreased relative to isocentre. The polarity of the current flowing through the coil determines which end of the

gradient is higher than isocentre (positive) and which end is lower (negative). Gradient coils are powered by gradient amplifiers. There are two gradient amplifiers for each gradient, one affixed to the high end of the gradient, the other to the low. [7]

2.4.4 Shimming coil:

Shimming coil is used in the process of balancing the main magnetic field. Shimming coil is critical to the maintenance of homogeneity. It reduces residual inhomogeneity as well as patient induced inhomogeneity. [7]

2.4.5 Computer system in MRI:

Currently, every MRI system has a minimum of two computers. The main or host computer controls the user interface software. Software enables the operator to control all functions of the scanner either directly or indirectly. The second computer system is a dedicated image processor used for performing the Fourier transformations or other processing of the detected data. [7]

2.5 Artifacts of MRI:

An artifact is something that appears in an image and is not a true representation of an object or structure within the body [8]

Artifacts are misrepresentations of tissue structures seen in images produced by MRI. Examples are:

- Chemical shift.
- Chemical misregistration.
- Magnetic susceptibility.
- Aliasing.
- Phase mismapping .[9]

2.5.1 Chemical shift:

Chemical shift artifact is a displacement of signal between fat and water along the frequency axis of the image. An example is around the kidneys where the water-filled kidneys are surrounded by peri-renal fat. To avoid this artifact MRI operator has to:

- Scan with a low field strength magnet.
- Broaden the receive bandwidth. [9]

2.5.2 Chemical misregistration:

Chemical misregistration is caused by the difference in precessional frequency between fat and water that results in their magnetic moments being in phase with each other at certain times and out of phase at others.

This artifact mainly occurs along the phase axis and causes a dark ring around structures that contain both fat and water. To reduce this artifact MRI operator has to Use Spin Echo (SE) or Fast Spin Echo (FSE) pulse sequences (which use RF, re-phasing pulses). [9]

2.5.3 Magnetic susceptibility:

The magnetic susceptibility of a substance is the ability of external magnetic fields to affect the nuclei of a particular atom, and is related to the electron configurations of that atom. Magnetic susceptibility artifact occurs because all tissues magnetize to a different degree depending on their magnetic characteristics. To eliminate this artifact MRI operator has to:

- Use Spin Echo or Fast Spin Echo pulse sequences (which use RF rephasing pulses).
- Removing all metal items from the patient before the examination. [9]

2.5.4 Aliasing:

This occurs when anatomy that is producing signal exists outside Field of View (FOV) in the phase direction. Anatomy from one side of the image overlaps the other. To eliminate or reduce the aliasing, one has to increase the FOV to the boundaries of the coil. [9]

2.5.5 Phase mismapping:

Phase artifact results from anatomy moving between the application of the phase encoding gradient and the frequency encoding gradient (intra-view) and motion between each application of the phase gradient (view to view). If anatomy moves during these periods it is assigned the wrong phase value and is mismapped onto the image. It causes an artifact called phase mismapping and always occurs along the phase axis of the image. This artifact appears as blurring or ghosting across the image. This artifact is eliminated by:

- Changing the phase and frequency direction removes the artifact from the area of interest.
- Designing a system to detect the patient motion, and this is the objective of the project. [9]

2.6 K-space" data acquisition and image reconstruction

2.6.1 K-space matrix

- MR data are initially stored in the k-space matrix fig (2.3), the "frequency domain" repository [10]
- The axes have units of cycles/unit distance
- Each axis is symmetric about the center of k-space, ranging from –fmax to +fmax

Low-frequency signals are mapped around the origin of k-space and high frequency signals are mapped further from the origin in the periphery

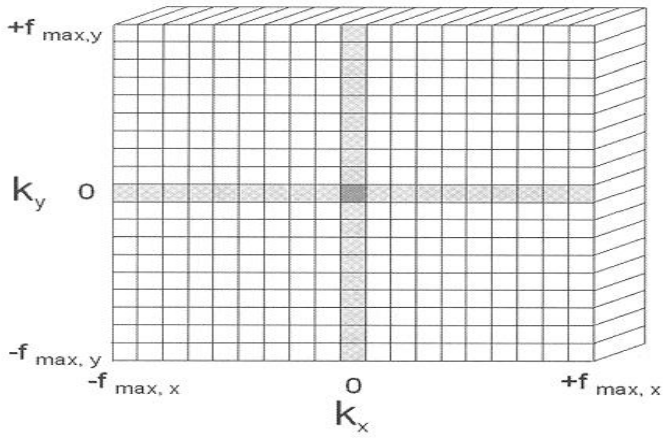

Figure 2.3 matrix of MRI.

- Frequency domain data are encoded in the kx direction by the frequency encode gradient (FEG), and in the ky direction by the phase encode gradient (PEG) in most image sequences
- Lowest spatial frequency increment is the bandwidth across each pixel [10]

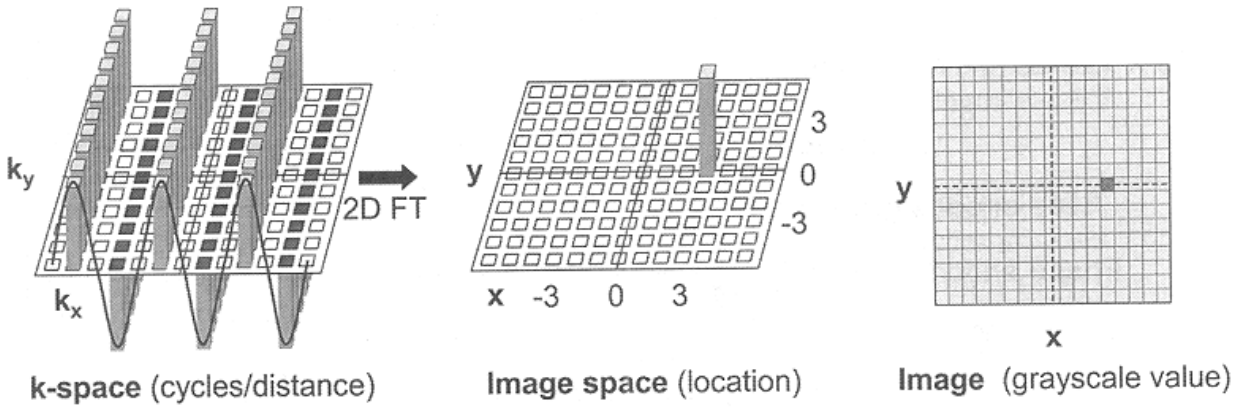

Figure 2.4 k-space distance, location, gray scale.

2.6.2 Two-dimensional data acquisition:-

- MR data acquired as a complex, composite frequency waveform
- With methodical variations of the PEG during each acquisition fig (2.5), the k-space matrix is filled to produce the desired variations across the frequency and phase encode directions [10]

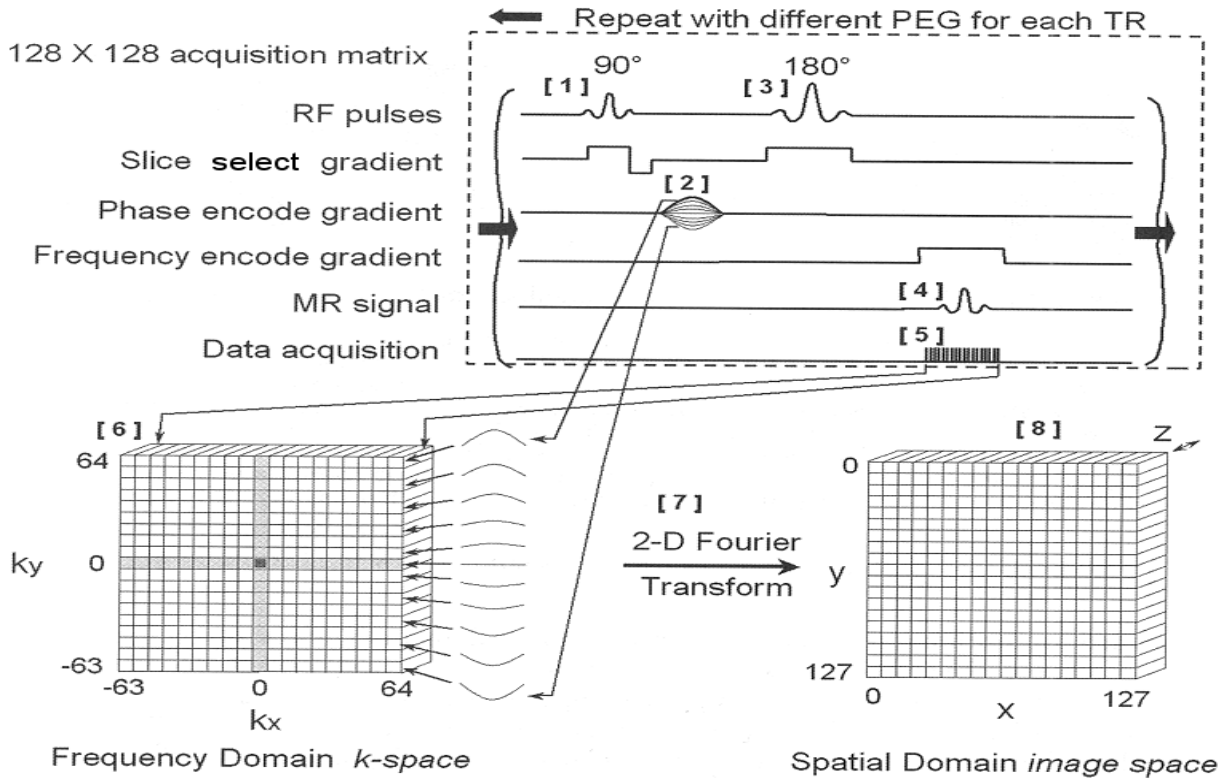

Figure 2.5 MRI pulse sequence.

1. Narrow band RF excitation pulse applied simultaneously with the slice select gradient (SSG)
    - Energy absorption dependent on amplitude and duration of the RF pulse at resonance
    - Longitudinal magnetization converted to transverse magnetization, extent of which depends on saturation of spins and angle of excitation

- 90-degree flip angle produces maximal transverse magnetization

2. Phase encode gradient (PEG) applied for a brief duration to create phase difference among spins along the phase encode direction

- Produces several "views" of the data along the ky axis, corresponding to the strength of the PEG

3. Refocusing 180-degree pulse delivered after selectable delay time, TE/2

Inverts direction of individual spins and reestablishes phase coherence of transverse magnetization with formation of echo at time TE

4. During echo formation and subsequent decay, frequency encode gradient (FEG) applied orthogonal to both slice select and phase encode gradient directions
    - Encodes precessional frequencies spatially along the readout gradient
5. Simultaneous to application of FEG and echo formation, computer acquires the time-domain signal using an analog-to-digital converter (ADC)
    - Sampling rate determined by excitation bandwidth
    - One-dimensional Fourier transform converts the digital data into discrete frequency values and corresponding amplitudes

Proton precessional frequencies determine position along the k_x (readout) direction

6. Data deposited in k-space matrix in a row, specifically determined by the PEG strength applied during excitation
    - Incremental variation of the PEG throughout the acquisition fills the matrix one row at a time

- Possible to acquire the phase encode data in nonsequential order to fill portions of k-space more pertinent to the requirements of the exam (e.g., in low-frequency, central area of k-space)
- After matrix is filled, columns contain positionally dependent phase change variations along the KY (phase encode) direction

7. Two-dimensional inverse Fourier transform decodes the frequency domain information piecewise along the rows and then along the columns of k-space

8. Final image is a spatial representation of the proton density, T_1, T_2, and flow characteristics of the tissue using a gray-scale range

- Each pixel represents a voxel; thickness determined by slice select gradient strength and RF frequency bandwidth [10]

2.7 Classification of Motion in MRI according to the acquisition blocks

2.7.1 intrashot-motion

- Motion present during acquisition blocks
- Effects: determined by presence of field gradients! Additional signal Phase; corrupted excitation profile. [11]

2.7.2 intershot-motion

- Motion present between acquisition blocks
- Approximation: motion state changes only with the phase encoding
- (Cartesian sampling) [11]

2.8 classification of motion according to the human body Rigid/non-rigid motion

2.8.1 rigid-motion

- Translation: Fourier-shift-theorem
- Rotation: Fourier-rotation theorem
- Rigid motion manifests itself in blurring and ghosting
- Head-motion, arm-motion, leg-motion

2.8.2 non-rigid-motion

- Hard to determine, cardiac-motion, respiration, gastrointestinal Peristalsis, pulsatile brain-motion

2.9 Correction Approaches

2.9.1 Prospective Motion Correction:

E.g. PROMO, real-time gradient adjustment, gating, triggering

2.9.2 Retrospective Motion Correction:

Mathematical approaches focusing on data consistency

2.9.3 Data Acquisition Strategies:

E.g. PROPELLER sequence, radial/spiral sampling, fast-imaging techniques [11]

2.10 Image restoration

Image restoration is one of the fundamental problems in image processing. It aims at reconstruction of true image from the degraded image. There are two main kinds of blurring: one is motion blur, which is caused by the relative motion

between the camera and object during image capturing; the other is defocus blur, which is due to the inaccurate focal length adjustment at the time of image capturing. Blurring induces the degradation of image quality, specifically for sharp images where the high frequency information can be easily lost due to blur. An image restoration technique refers as non-blind restoration, if blur kernel information is available. In case of blind restoration, blur kernel information is not known. Blind image restoration problem has been categorized into two groups. In the first group, we can put those methods in which the point spread function (PSF) of blur is estimated in first step and then degraded image is restored using any of the classical deconvolution methods such as wiener or inverse filtering in subsequent step. In the methods of second group, PSF estimation and image restoration are achieved simultaneously [12].

CHAPTER THREE

3. LITERATURE REVIEW

The MRI image motion correction goes through three main methods this chapter will discuss some papers were published during the last fifteen years.

3.1 Prospective Motion Correction real time motion correction.

"A paper describes Prospective Acquisition Correction for Head Motion with Image-based Tracking for Real-Time fMRI 2000, [13]"

A prospective Acquisition Correction for Head Motion with Image-based Tracking for Real-Time fMRI. Scanning and processing of data were performed on a standard MAGNETOM Symphony 1.5T MR system (Siemens, Erlangen, Germany). For image acquisition a 2D single shot EPI and a fast RF-spoiled gradient echo sequence (FLASH) were programmed with full oblique and off-center functionality for all axes. Calculation of complete sequence timing including the physical gradient pulses is performed on the fly within 3 milliseconds prior to each scanned volume. So real-time adjustment of position and orientation of the slice stack is possible. The system allows real-time reconstruction of the data using the imaging computer. For further evaluation of the images, the data are transferred to the host computer. Here a motion detection algorithm related to the method introduced by Friston et al. (4,5) is applied, estimating a three dimensional rigid body transformation against a reference volume. The new positional information is passed to the measurement computer, which adjusts the parameters for slice orientation and position for the next acquisition. In this implementation the positional information is fed back with a temporal delay of one acquisition cycle, which is about 4 seconds in usual 2D multi-slice EPI based MRI measurements.

Clinical datasets show that the residual scan to scan motion is commonly smaller than 50mm and so almost negligible in the most cases. Thus fine adjustment of the residual motion is performed by the real-time application of additional retrospective correction of the volumes with Fourier interpolation.

Contributions of this work has a high stability and accuracy involving real-time motion correction. An unmodified commercial MRI scanner was used, so the clinical use of PACE is possible. Benefits of the PACE technique can be visualized by examination of difference images. Significant decrease of variance when the PACE method was used in comparison to retrospective techniques.

This technique has a clear draw back because of using again the retrospective method to correct the residual motion which some data may loss. And this adds some complexity in procedure.

"A paper introduces - Prospective motion correction of high-resolution magnetic resonance imaging data in children 2010, [14]"

This method attempts to address the problem of motion at its source by keeping the measurement coordinate system fixed with respect to the subject throughout image acquisition. The technique also performs automatic rescanning of images that were acquired during intervals of particularly severe motion. Unlike many previous techniques, this approach adjusts for both in-plane and through-plane movement, greatly. Imaging data were obtained at the UCSD Radiology Imaging Laboratory on a 1.5 Tesla GE Signa HDx 14.0M5 Twin Speed system (GE Healthcare, Waukesha, WI) using an eight-channel phased array head coil. Acquisitions included a conventional three-plane scout and a set of four 3D inversion recovery spoiled gradient echo (IR-SPGR) T1-weighted volumes with pulse sequence parameters optimized for maximum gray/white matter contrast (TE=3.9 ms,

TR=8.7 ms, TI=270 ms, flip angle=8°, TD=750 ms, bandwidth=±15.63 kHz, FOV=24 cm, matrix=192×192, voxel size=1.25×1.25×1.2 mm). The sequences used for the four T1 images were identical except that PROMO motion tracking and correction was turned off for two scans and on for the other two, in alternating fashion. The order of scanning for the four T1 scans was counterbalanced across subjects, with four participants undergoing a sequence of on–off–on–off and five undergoing off–on–off–on.

Real-time motion tracking and correction with spiral navigator (SNAV) sequences was performed using the extended Kalman filter (EKF) algorithm (Gelb, 1974) applied to MRI as reported by Dale and colleagues (White et al., 2007, 2010) and as described previously for prospective motion correction in S-NAV 3D pulse sequences (Roddey et al., 2008;Shankaranarayanan et al., 2007). Five sets of three orthogonal low flip, single shot S-NAVs were interspersed within the dead time of all four 3D IR-SPGR T1 scans in order to measure and adjust for head movement while scanning (White et al., 2010). Of note, the placement of the S-NAV scans can vary according to the specific pulse sequence being used. Online navigator-derived motion measures were used to adjust the image coordinate system with respect to brain position and to automatically rescan images that were acquired during intervals with particularly high motion, as determined by the position difference between the two navigator scans that "sandwich" each partition. For this study, a rescan threshold was determined based on the noise level characteristics of a sample of "cooperative" adult subjects (i.e., who showed a relative absence of motion). Rescans were set to be triggered by a norm of 1 or greater in the motion measures during an acquisition (i.e., a norm of 1 mm of total translation or a norm of 1° of total rotation by any combination of the head position values. A rescan of the entire volume was allowed, if necessary according to subject movement. For images acquired without PROMO, scan duration was 8 min, 40 s per T1 volume.

The S-NAV/EKF framework offers the advantage of image based tracking within regions of interest that are specific to each subject, masking out motion from non-brain locations such as the neck and jaw, which can corrupt the motion estimates.

Motion estimates for the PROMO-enabled volumes were computed from navigator scans, tracking position as a six-element vector. As an index of each individual's magnitude of head motion, the norm of the range of motion measures (minimum to maximum) was computed across both PROMO-on scans for each subject for translation and rotation. This “Euclidean” (or L2) norm is a normalized measure of the magnitude of variability in motion—in this case the square root of the sum of squares of the range of motion—that has the advantage of being independent of relative position in the x, y, z coordinate space. Motion estimates were not calculated for the two PROMO-off scans, since tracking and correction was disabled.

The contributions In addition to improvements in quantitative measures, PROMO corrected volumes also were consistently rated subjectively as superior to uncorrected images for both overall clarity and reduced motion-specific artifacts. As with quantitative measures, qualitative ratings were better in all cases when PROMO was enabled. Although this particular study did not focus on clinical pulse sequences, our findings suggest that prospective motion correction would also be useful in standard clinical neuroradiological assessment and diagnosis.

Main drawbacks the number of rescans required because of subject movement, and therefore the additional time required for acquisition with PROMO enabled, also varied considerably among subjects. The additional acquisition time required for PROMO-on scans was on average 34.3 s per volume, but this varied widely and was heavily affected by one outlying individual; the median additional scan time was 7.5 s, the standard deviation was 69.4 s, and the duration ranged from 0 to 292.5 s (4 min, 52.5 s). The correlation coefficient (Pearson, one-tailed) between

the total number of rescans and head translation was r=0.72 (p=0.01) and between rescans and rotation was r=0.61 (p=0.04).

3.2 Retrospective Motion Correction mathematical approaches focusing on data consistency.

"A paper describe Image-Based Method for Retrospective Correction of

Physiological Motion Effects in fMRI: RETROICOR **2000, [15]"**

Simple MRI image-based motion correction method that does not have the limitations of k-space methods that preclude high spatial frequency correction. Low-order Fourier series are fit to the image data based on time of each image acquisition relative to the phase of the cardiac and respiratory cycles, monitored using a photo plethysmograph and pneumatic belt, respectively. The RETROICOR method is demonstrated using resting-state experiments on three subjects and compared with the k-space method. The method is found to perform well for both respiration- and cardiac-induced noise without imposing spatial filtering on the correction.

The correction method assumes that the time series of intensities y (t) in a pixel is corrupted by additive noise resulting from cardiac and respiratory functions. The cardiac and respiratory states are monitored during the scan using a photo plethysmograph and a pneumatic belt placed around the subject's abdomen, respectively. It is assumed that the physiological processes are quasi-periodic so that cardiac and respiratory phases can be uniquely assigned for each image in the time series. All experimental imaging data were obtained with a 3 T scanner equipped with high-performance gradients and receiver (GE Signa, rev 8.2.5, Milwaukee, WI). T1weighted FSE scans were acquired for anatomic reference

(TR/ spin-echo time (TE)/ETL 5 68 msec/4000 msec/12). An automated high-order shimming method based on spiral acquisitions was employed to reduce B0 heterogeneity. Resting-state "functional" acquisitions used a 2D spiral gradient-recalled echo sequence with TE 30 msec, field of view (FOV) 22 cm, and scan duration of 200 sec (8). The in-plane trajectory was a single-shot uniform-density spiral providing resolution of 2.3 mm (matrix 96 3 96). Either three or twelve 5 mm slices (depending on TR; see below) were acquired with axial scan plane. In Subject 3, oblique coronal planes nominally perpendicular to the calcarine fissure (often used when studying visual cortex) were also obtained. A homemade head coil was used for all scans and subjects were stabilized with foam padding packed tightly in the coil. Images were reconstructed into a 128 3128 matrix with an off-line computer (Sun Microsystems, Mountain View, CA) using gridding and fast-Fourier transforms (FFTs). Linear shim corrections for each slice were applied during reconstruction using individual field maps obtained during the scan. Two scans were obtained for each of three subjects at TRs of 250 msec (3 slices, 800 time frames each) and 1000 msec (12 slices, 200 frames). The shorter TR ensured that cardiac fluctuations in the images were resolved without temporal aliasing, whereas the longer TR provided more typical scan conditions in which cardiac pulsation could alias into spectral regions that overlap with those of the stimulus and respiration. The resting-state data were acquired with no intentional task, for which the subjects were instructed to keep their eyes closed.

The contributions of this work are: first, The RETROICOR method, in contrast with RETROKCOR, treats each pixel separately and therefore does not introduce artificial coupling of noise corrections across spatial regions. As a result, the RMS noise from cardiac and localized respiratory pulsatility was found to be reduced to a greater extent by the new method than by the k-space method. Second, that real-

image data rather than complex raw data are corrected, which reduces the computational burden by half. Furthermore, because it is a post processing method operating on images, it may be easier to apply in practice than the k-space method because it is not necessary to invoke an off-line reconstruction after the corrections are made. Main drawbacks an assumption of the image-based correction is that each image is collected at a discrete time for which unique cardiac and respiratory phases can be assigned. This is a good assumption for single-shot imaging, but may not hold for multishot acquisitions, because the multiple-TR periods needed for all segments may span several cardiac or respiratory cycles

"A paper propose Retrospective Motion Correction Protocol for High-Resolution Anatomical MRI 2006, [16]"

In this study a retrospective motion correction (RMC) were tested, common for functional MRI (fMRI) image motion correction, as a means to improve the quality of high-resolution 3-D anatomical MR images. RMC methods are known to be effective for correcting interscan retrospective motion correction algorithm is proposed, which significantly reduces ghosting and blurring artifacts due to subject motion. The technique of the raw data of standard imaging sequences was used; no sequence modifications or additional equipment such as tracking devices are required. Similar to other approaches, we assume that the motion time-scale is longer than the repetition time TR, i.e. we model the motion trajectory as a piecewise constant function. We neglect second order effects such as the influence of motion on the magnetic field. Like all other reference-free (no external information on motion) methods we assume that the imaged object behaves as a rigid body. Under these assumptions we can correct for arbitrary motion trajectories in 6 degrees of freedom for both 2D and 3D acquisitions. We provide a Matlab implementation of GradMC along with 4 examples.

First the motion corrupted k-space data was modeled. Next, the cost function based on the image gradient entropy metric was constructed. We then describe how translational and rotational motion was implemented, and deal with non-linearities and local minima in our objective using multiscale optimization. Finally, we demonstrate that our method can be extended to multiple coils.

The contributions the obvious and very strong advantage of our method (and retrospective methods in general) is that it can be applied to any already acquired dataset (subject to our model assumptions), and does not require the use of any tracking equipment, or special imaging sequences. By applying additional constraints, it may also be extendable to handle non-rigid body motion, for which prospective correction is highly challenging.

Main drawbacks the current major limitation of the method was the inability to correct for motion involving strong rotations (angles larger than 3°). The visual quality of a reconstructed image never gets worse than that of a degraded image, however, the stronger the rotation, the less improvement can be achieved. For rotation angles larger than 10°, the corrected image looks essentially the same as the degraded one. A strong assumption we make is that the imaged object behaves as a rigid body. Indeed, this is what allows us to carry out fast multiplications with the matrix A_ in the Fourier domain. Slight deviations from non-rigidity are well tolerated, however gross effects (e.g. due to movement of the tongue during the acquisition) make an artifact-free correction difficult. We also assume that the input to Grad MC is the raw k-space data along with the order in which the k-space was sampled. In a clinical setting, such data is not always available, because often only magnitude images are preserved. Since real data from the scanner often has non-uniform spatial phase

“A paper propose Blind Retrospective Motion Correction of MR Images 2007. [17]”

Another retrospective motion correction algorithm is proposed, which significantly reduces ghosting and blurring artifacts due to subject motion. The technique uses the raw data of standard imaging sequences; no sequence modifications or additional equipment such as tracking devices are required. Similar to other approaches, we assume that the motion time-scale is longer than the repetition time TR, i.e. we model the motion trajectory as a piecewise constant function. We neglect second order effects such as the influence of motion on the magnetic field. Like all other reference-free (no external information on motion) methods we assume that the imaged object behaves as a rigid body. Under these assumptions we can correct for arbitrary motion trajectories in 6 degrees of freedom for both 2D and 3D acquisitions. We provide a Matlab implementation of GradMC along with 4 examples. first the motion corrupted k-space data was modeled. Next, we construct the cost function based on the image gradient entropy metric. We then describe how translational and rotational motion is implemented, and deal with non-linearities and local minima in our objective using multiscale optimization. Finally, we demonstrate that our method can be extended to multiple coils.

The contributions the obvious and very strong advantage of our method (and retrospective methods in general) was that it can be applied to any already acquired dataset (subject to our model assumptions), and does not require the use of any tracking equipment, or special imaging sequences. By applying additional constraints, it may also be extendable to handle non-rigid body motion, for which prospective correction is highly challenging.

The major limitation of our method is the inability to correct for motion involving strong rotations (angles larger than 3°). The visual quality of a reconstructed image

never gets worse than that of a degraded image, however, the stronger the rotation, the less improvement can be achieved. For rotation angles larger than 10°, the corrected image looks essentially the same as the degraded one. A strong assumption we make is that the imaged object behaves as a rigid body. Indeed, this is what allows us to carry out fast multiplications with the matrix A_ in the Fourier domain. Slight deviations from non-rigidity are well tolerated, however gross effects (e.g. due to movement of the tongue during the acquisition) make an artifact-free correction difficult. We also assume that the input to Grad MC is the raw k-space data along with the order in which the k-space was sampled. In a clinical setting, such data is not always available, because often only magnitude images are preserved. Since real data from the scanner often has non-uniform spatial phase

3.3 Data Acquisition Strategies: e.g. PROPELLER sequence, radial/spiral sampling, fast-imaging techniques

"A paper describe Periodically Rotated Overlapping Parallel Lines with Enhanced Reconstruction 2011, [18]"

A PROPELLER MRI data was collected in such a way that can mitigate the (in-plane motion, phase inconsistencies, and through-plane motion). This approach can be blended with many techniques, and has been successfully implemented with gradient echo and turbo spin echo sequences. Data are collected in k-space in N strips, each consisting of L parallel lines, corresponding to the L lowest phase encoded lines in any Cartesian-based data collection.

Each strip is rotated in k-space by an angle $\bar{\alpha} = \pi / N$., so that the total Rotated, overlapping strips in k-space. Data set spans a circle in k-space. If a matrix

diameter of M is desired, then Land N are chosen so that $L N = M \pi / 2$. The central circle in k-space with diameter L is collected for each of the N strips; these are used to form N low-resolution images, which are compared to each other to remove in-plane displacement and phase errors that are slowly varying spatially. These factors are corrected for each strip.

Cross-correlation measures between the low resolution images are used to determine which strips were collected with significant through-plane displacement. As the data are combined in k-space, the data from strips with the least amount of through-plane motion are preferentially used in regions of strip overlap, thus reducing artifacts from through-plane motion.

The contributions of this work are: removal of respiratory motion from ECG gated cardiac MRI, allowing breath hold-quality images without breath holding Motion correction was performed using only a limited FOV around the heart in the low-resolution images.

Main drawbacks successfully only with gradient echo and turbo spin echo sequences. Increase in overall imaging time (due to strip overlap) and a loss of information at the corners of k-space.

“A paper describe Motion Correction with Propeller MRI: Application to Head Motion 2010, [19]”

The PROPELLER MRI (Periodically Rotated Overlapping Parallel Lines with Enhanced Reconstruction) was implemented as a new technique in data collection and reconstruction. The data is collected in concentric rectangular strips that rotate around the k space. The central portion is contained in each strip and therefore can be used to obtain a low frequency average image It can compensate for the phase and bulk translation, rotation and scaling in the image. Moreover it can further

reject data which has significant motion based on a correlation measure. Methods which collect data from center to outwards of k space such as projection reconstruction and spiral MRI reduce these motion artifacts by oversampling the central k-space which can be thought as an analogy of averaging the data in conventional imaging. Other methods try to estimate the motion or motion related phase from extra collected data which are referred as navigator echoes. They generally compute the bulk transformation in the data and correct for these artifacts in the image.

Phase Correction: In this step, we correct the small displacement in the k-space due to the imperfect gradient of MRI machine. The basic idea is to remove the low frequency part of the reconstructed image phase by a pyramid triangle window.

Bulk Transformation Correction: After doing the phase correction of the data we estimated the bulk transformation of the object between each strip and corrected for these artifacts. If we restrict our model to affine case the bulk transformation are caused by rotation, translation and scaling. These transformations have nice one to one Fourier transform correspondences. In our approach we estimated each transformation separately.

Bulk Translation Correction: From the Fourier Transform theory we know that translation in image space causes some linear phase shifts in its Fourier transform. Therefore, the linear phase shift can be corrected by estimating the translation in image space.

Bulk Scaling Correction:

As rotation and translation in image space have corresponding properties in Fourier space, a similar relation is also observed with the scaling in the image space. Scaling in image space also causes scaling in Fourier space. However this scaling

is inversely proportional such that contraction in one domain produces corresponding expansion in the other domain. (Equation 3). Therefore, the scaling factor in image space can be directly computed using the k-space data as done in rotation case. Correlation Weighting: some strips will still have factors that will produce artifacts because of the significant inter-plane motion after doing all the previous corrections. We can calculate a weight of each strip based on the correlation, and then multiply the data of each strip by this weight to compensate for these artifacts.

The contributions of this work that the registration correction works very well. Looking at the original images that were reconstructed from each strip we do not see much registration errors. Therefore there have been little changes after rotation, translation and scaling corrections

Main drawbacks the excessive oversampling of the center of k-space and neglect the hall. K-space is one of the main dis advantages which affect the producing image. Second the assumption that motion is rigid since we use head data, the movements are restricted only to rigid case

"A paper propose different method MRI with TRELLIS: which is a novel approach to motion correction 2012, [20]"

This was provide a full description of the TRELLIS k-space trajectory and reconstruction algorithm. Results from computer simulations, a physical 'moving phantom' and a human subject are presented. Through comparison with existing methods. K-Space is filled using orthogonal overlapping strips and the directions for phase- and frequency-encoding are alternated such that the frequency-encode direction always runs lengthwise along each strip. The overlap between strips is used both for signal averaging and to produce a system of equations that, when

solved, quantifies the rotational and translational motion of the object- an acronym for Translation and Rotation Estimation using Linear Least-squares and Interleaved Strips and so named because its sampling pattern looks like a trellis. Results obtained from simulations with computer-generated phantoms, a purpose-built moving phantom, and in human subjects show the method is effective. TRELLIS offers some advantages over existing techniques in that k-space is sampled uniformly and all acquired data are used for both motion detection and image reconstruction. This technique has some similarities to PROPELLER: it does not require extra hardware; it samples k-space more than once in order to obtain information about patient motion; and the final reconstruction requires some form of gridding.

The contributions of TRELLIS may offer significant advantages because the whole of k-space is uniformly sampled instead of concentrating sampling in the center of k-space as in PROPELLER. Therefore all collected data are used for both motion detection and image reconstruction and excessive oversampling of the center of k-space is avoided. It is likely, however, that this advantage is gained at a cost of decreased motion detection accuracy compared to PROPELLER. It is interesting to note that the TRELLIS sequence is relatively robust to motion even without the application of motion correction performed in post-processing.

Main drawbacks. TRELLIS may have some problem multishot diffusion-weighted sequences. Strip in H and V lies directly over the center of k-space (Fig. 10B). The advantage is that the center of k-space will always be kept intact, no matter what motion occurred during imaging. Currently, ‘holes’ in k-space near the origin caused by a gap between strips after rotation correction can occasionally cause artifacts. The optimum width of each strip has also yet to be found. No assumptions are made about the nature of the motion as a function of time.

Incorporating prior knowledge of the maximum possible values of velocity or acceleration.

CHAPTER FOUR

4. METHODOLOGY

This chapter introduces the research methods that were used for this thesis including the main algorithm and the motion blur angle estimation algorithm and motion blur length estimation, were discussed in details, then Hough transform, cepstral method and wiener filter theories were demonstrating.

4.1 The methodology proceeds as follows:

first Appling Hough transformer function to the motion blurred image (Ifbl), to prepare motion angle estimation by building up the accumulator array.

Second Estimate the motion blur angle (THETA) using function that takes image as input and returns a collection of possible blur angles using step2 and other functions.

Third Estimate the length of the motion blur (LEN) which is the number of pixels by which the image is blurred the estimation depend on step2 beside other functions

Forth Prepare the wiener filter algorithm using the estimation of angle and length of the motion blur and SNR as parameters.

Fifth Starting motion blur correction by calling THETA value and LEN value and wiener filter function

Sixth The resulted corrected images according to different THETA and LEN estimation was displayed with better appearance in the blurred pixels.

Seventh the corrected image suffering some blur in the whole image sharping process are applied for better appearance

Eighth SNR calculated for the input images and the output image in order to verify which estimate THETA and LEN are result in better motion blur correction and to verify wiener filter validation in motion blur correction.

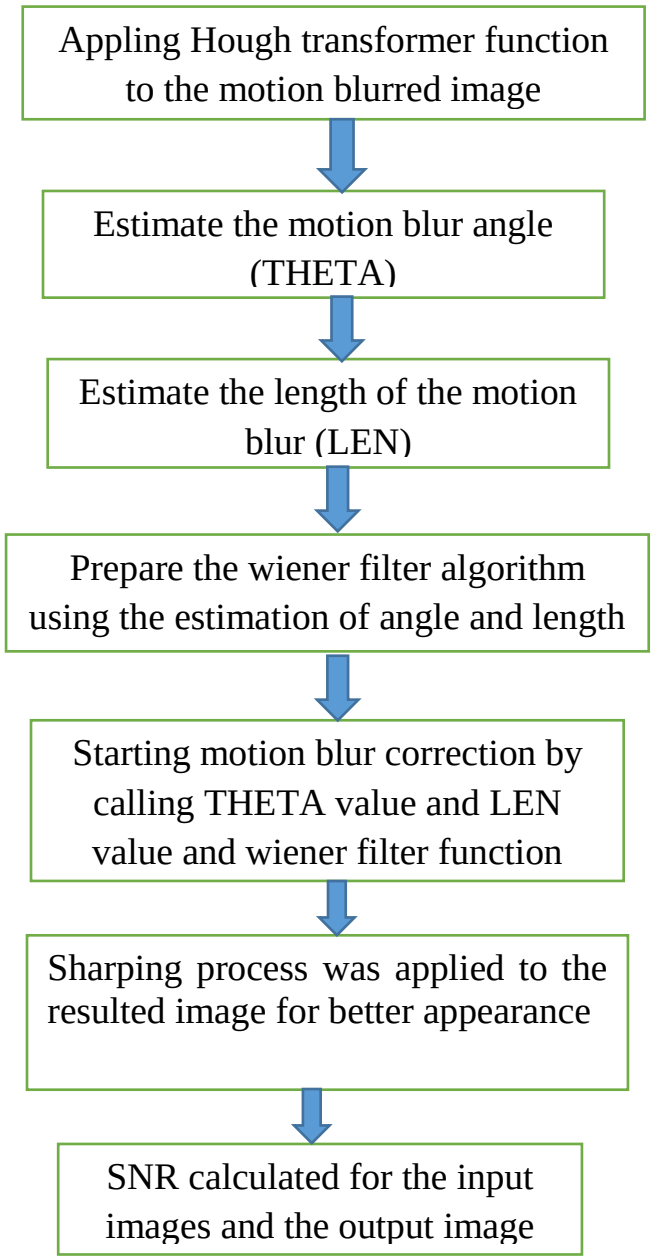

Block diagram 4.1 illustrate the main methodology process

4.2 Motion Blur Angle Estimation Algorithm

a) Performing Median Filter before restoring the blurred image and Display the input image.
b) Converting image from spatial domain to frequency domain.
c) Compute the log spectrum of F (u, v).
d) Convert the image to Cestrum (spectrum (IFT)) domain Compute the inverse Fourier transform of log spectrum.
e) Finding the edge map of the image in cepstral domain of step d.
f) Let theta min and the theta max be the minimum and maximum values of the motion blur angle.
g) Calling Hough transform to initialized the accumulator array.
h) Finding first maximum in the accumulator.
i) Storing first maximum in the array.
j) Saving the original accumulator array.
k) . Find the peak in Hough transform (the maximum value in accumulator array) which is perpendicular to the motion blur angle.
l) Iterating 10 times to find 10 highest angle values.
m) Calculate the possible values of THETA

4.3 Motion Blur Length Estimation Algorithm

a) Performing Median Filter before restoring the blurred image and Display the input image.
b) Converting image from spatial domain to frequency domain.
c) Compute the log spectrum of F (u, v).
d) Convert the image to Cepstrum (spectrum (IFT)) domain Compute the inverse Fourier transform of log spectrum.

e) Rotate the cepstral by the estimated angle in the inverse direction.
f) Convert the 2-D matrix of step e to 1-D by taking the averages of columns.
g) Find the distance of first negative peak from the origin which is corresponding to motion length.
h) If Zero Crossing found then return it as the blur length
i) If Zero Crossing not found then find the lowest peak Calculating the blur length using Lowest Peak

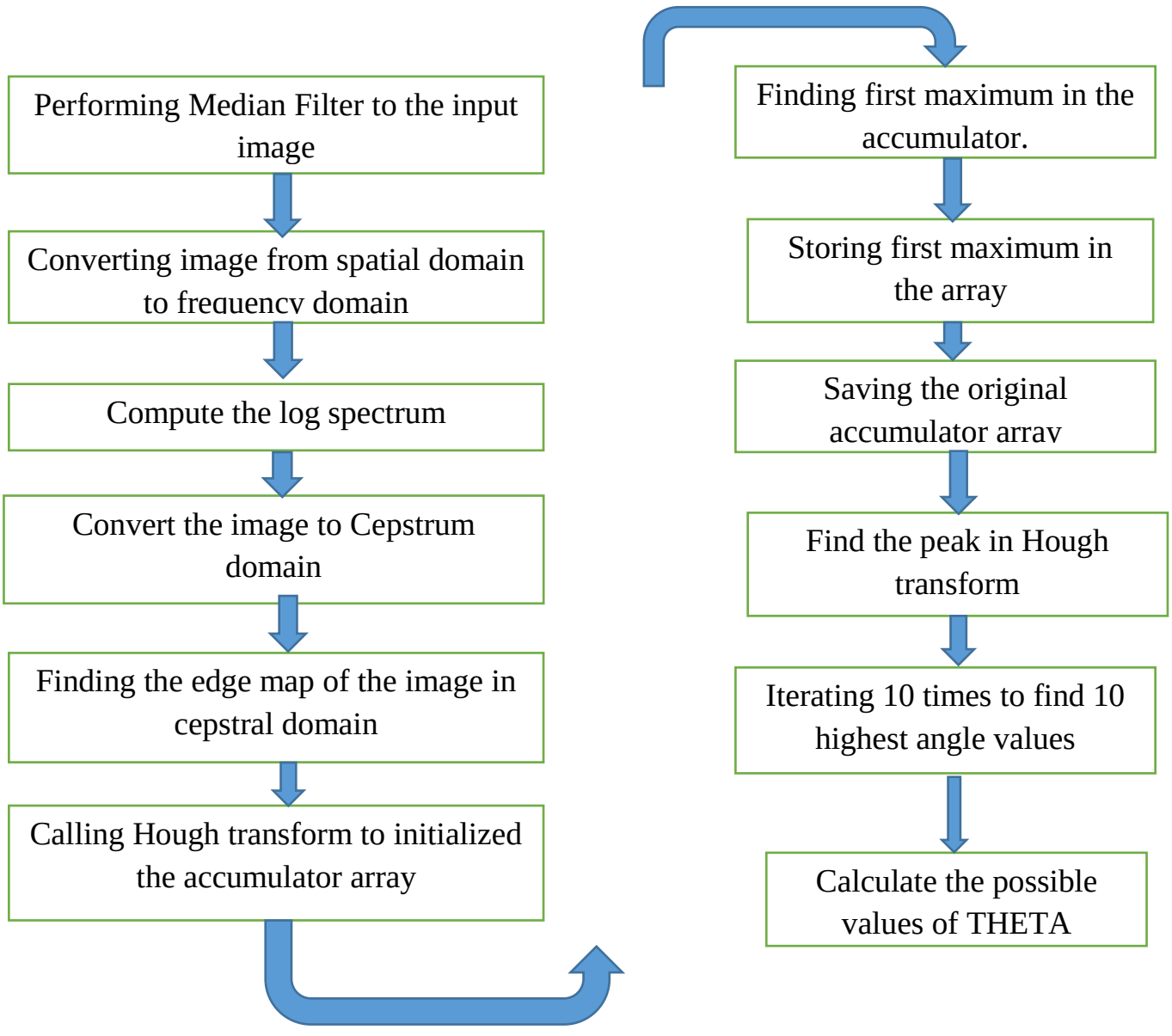

Block diagram 4.2 illustrate motion Blur Angle Estimation Algorith

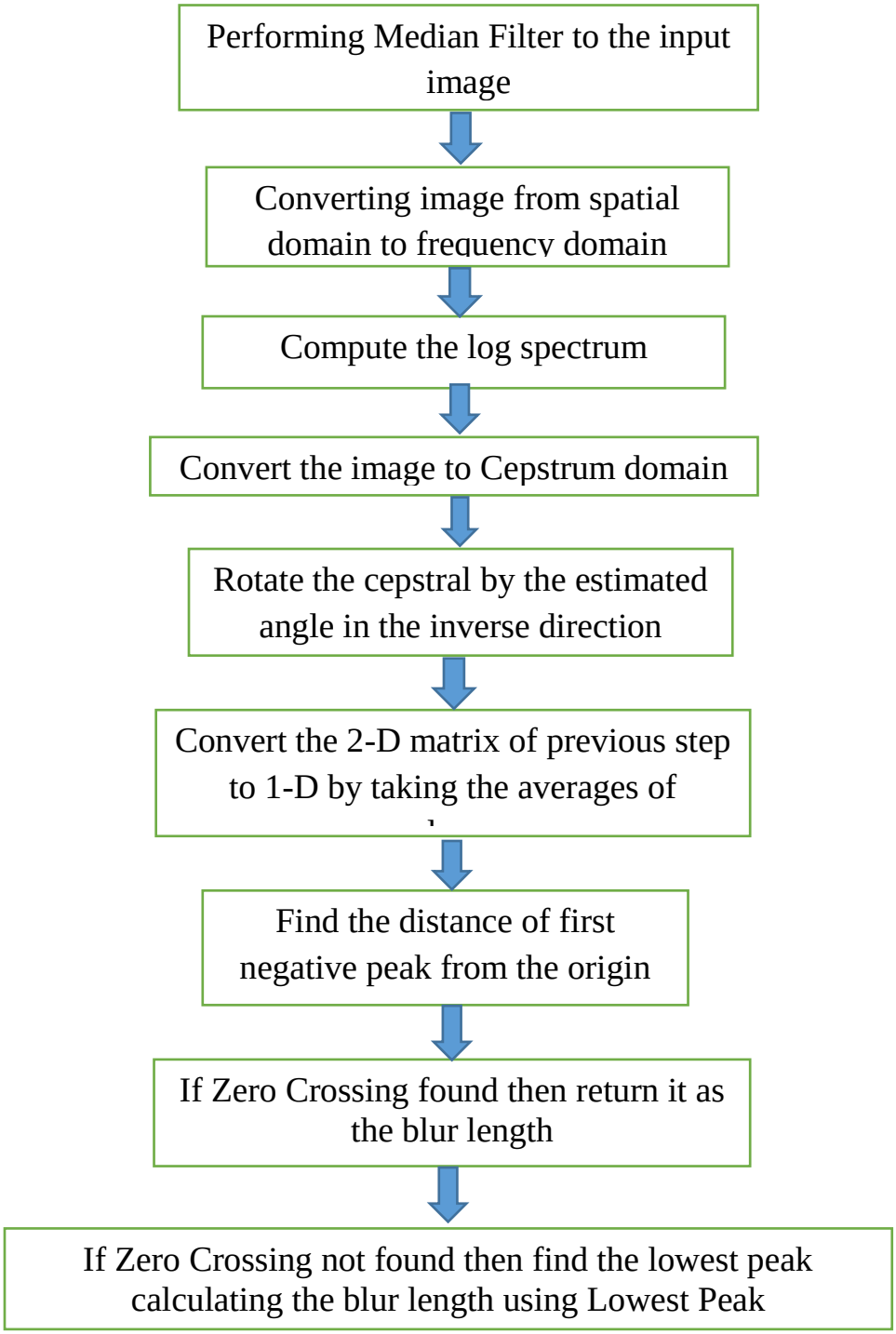

Block diagram 4.3 illustrate motion Blur length Estimation Algorithm

4.4 Hough Transform Method

The Hough transform [21] can be applied to find global patterns such as lines, circles, and ellipses in an image in a parameter space. It is especially useful in line detection because lines can be easily detected as points in Hough transform space, based on the polar representation of line given by (Equ. 4.1):

$$\rho = x\cos\theta + y\sin\theta \qquad 4.1$$

Where (X, Y) are Cartesian coordinates of a point on the line; θ is the angle between the perpendicular from the origin to the given line and the x-axis and ρ is the length of the perpendicular. Thus, a pair of coordinates (ρ, θ) can describe a line in polar domain. Fig. 4.1 shows transformation of line parameters from image domain to polar domain.

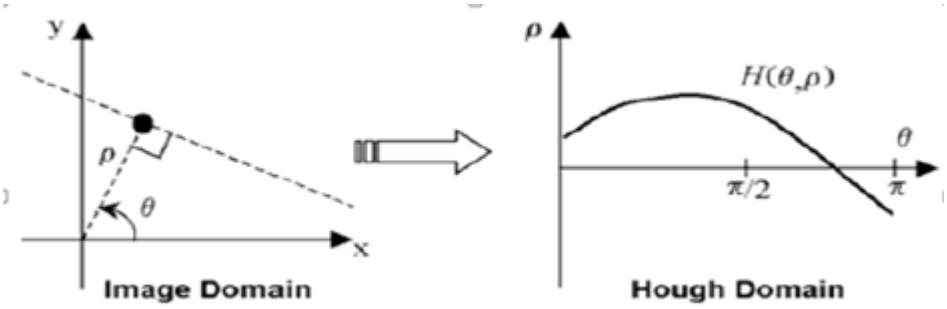

Figure 4.1 hough transform

The blur direction is obtained by locating the maximum value of this accumulator array. The Θ value corresponding to the maximum value of the accumulator array is the angle perpendicular to the blur direction. True blur direction is given by 900 - 0.

4.5 Cepstral Method

Cepstrum transform [21] can be used for separation of blur components and image components. Cepstrum transform of an image f(x, y) is defined in Equ(4.2) as follows: $\pi C \{f(x,y)\} = F\text{-}1(\text{Log}) \left| F(f(x,y)) \right|$ 4.2

Uniform motion blur in Frequency domain has periodic patterns by zero crossing of sinc function. Periodic patterns make negative peaks in cepstrum domain. Fig 4.2 shows cepstrum of blurred image has the negative peaks that are arisen by motion blur. For an estimated angle, we can estimate the blur length in an image. With the image in the cepstrum domain, first rotate the image by the expected blur angle and then take the average of each column to collapse 2-D cepstral into 1-D. By finding the number of columns between origin and first negative peak, we are able to find the periodicity and estimate the blur length for a given angle.

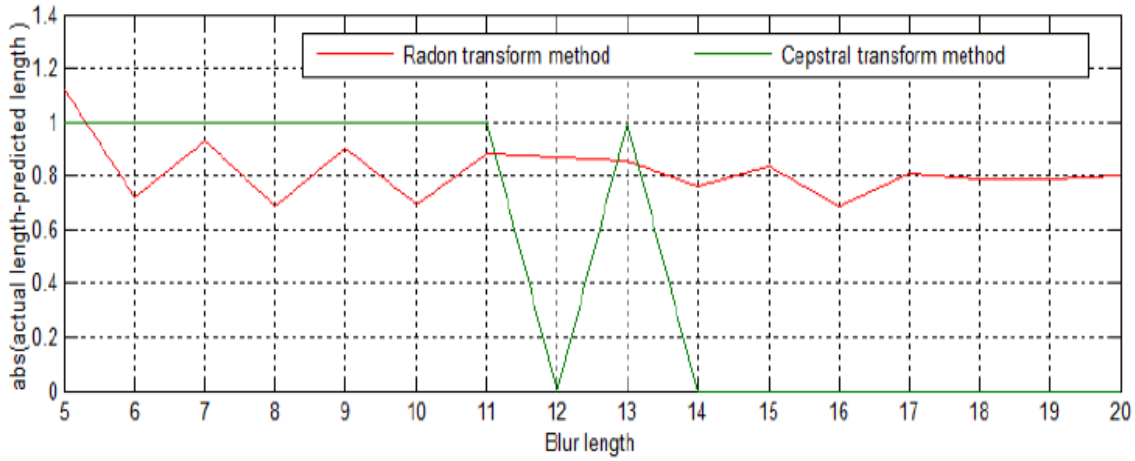

Figure 4.2 cepstral transform method

4.6 Wiener Filtering

Wiener filtering (after N. Wiener, who first proposed the method in 1 942) is One of the earliest and best known approaches to linear image restoration. A

Wiener filter seeks an estimate $\hat{f}$ that minimizes the statistical error function Equ(4.3)

$$e^2 = E\{(f - \hat{f})^2\} \qquad 4.3$$

Where E is the expected value operator and f is the undegraded image [22].

Description

J = deconvwnr(I,PSF,NSR) deconvolves image I using the Wiener filter algorithm, returning deblurred image J. Image I can be an N-dimensional array. PSF is the point-spread function with which I was convolved. NSR is the noise-to-signal power ratio of the additive noise. NSR can be a scalar or a spectral-domain array of the same size as I. Specifying 0 for the NSR is equivalent to creating an ideal inverse filter.

The algorithm is optimal in a sense of least mean square error between the estimated and the true images.

J = deconvwnr (I, PSF, NCORR, ICORR) deconvolves image I, where NCORR is the autocorrelation function of the noise and ICORR is the autocorrelation function of the original image. NCORR and ICORR can be of any size or dimension, not exceeding the original image. If NCORR or ICORR are N-dimensional arrays, the values correspond to the autocorrelation within each dimension.
If NCORR or ICORR are vectors, and PSF is also a vector, the values represent the autocorrelation function in the first dimension. If PSF is an array, the 1-D autocorrelation function is extrapolated by symmetry to all non-singleton dimensions of PSF. If NCORR or ICORR is a scalar, this value represents the power of the noise of the image [23].

CHAPTER FIVE

5. RESULTS AND DISCUSSION

A new method for MRI motion blur correction on the personal computer (PC) side using MATLAB program had been developed, the resulted images and the measured values will be discus in this chapter

To assess the overall impact of the using wiener filter in MRI image motion blur, the expected motion blur angle and motion blur length were estimated for more details Hough transform was used in line detection, ten different expected angles and length of motion blur were estimated.

According to the different measured angles and lengths motion correction was applied by wiener filter ten times, the resulted images were treated by sharpening filters and SNR were measured for all corrected image in order to compare which estimated angle and length were result a better a pperance.

For the ten different motion blur angles and lengths in coronal brain MRI image, the correction method results illustrated in the following figures, every one figure include the original image beside the corrected image in order to compare the different angles and length values restoration and their effect in the original corrupted image.

Then the same algorithm has been used for another sagittal and axial MRI motion blur image and the resulted corrected image has been illustrated following the coronal image figures, different angle and length for motion blur images has been estimated and accordingly different result was observed.

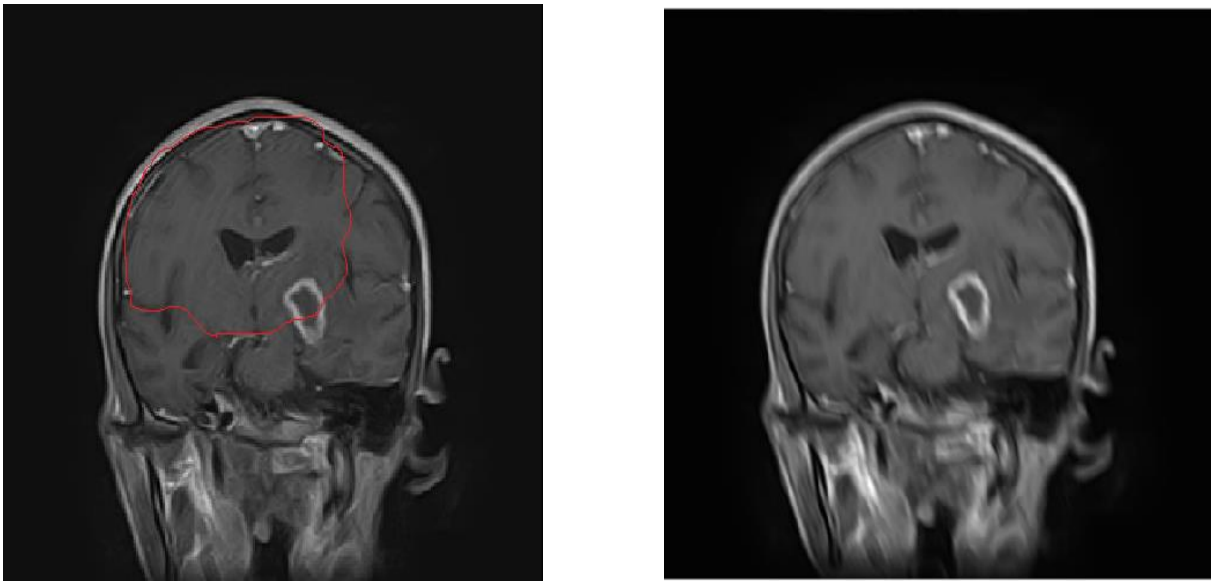

Figure 5.1 Comparison between the original coronal MRI image (L) and the corrected image(R) with angle 112° and length 11.

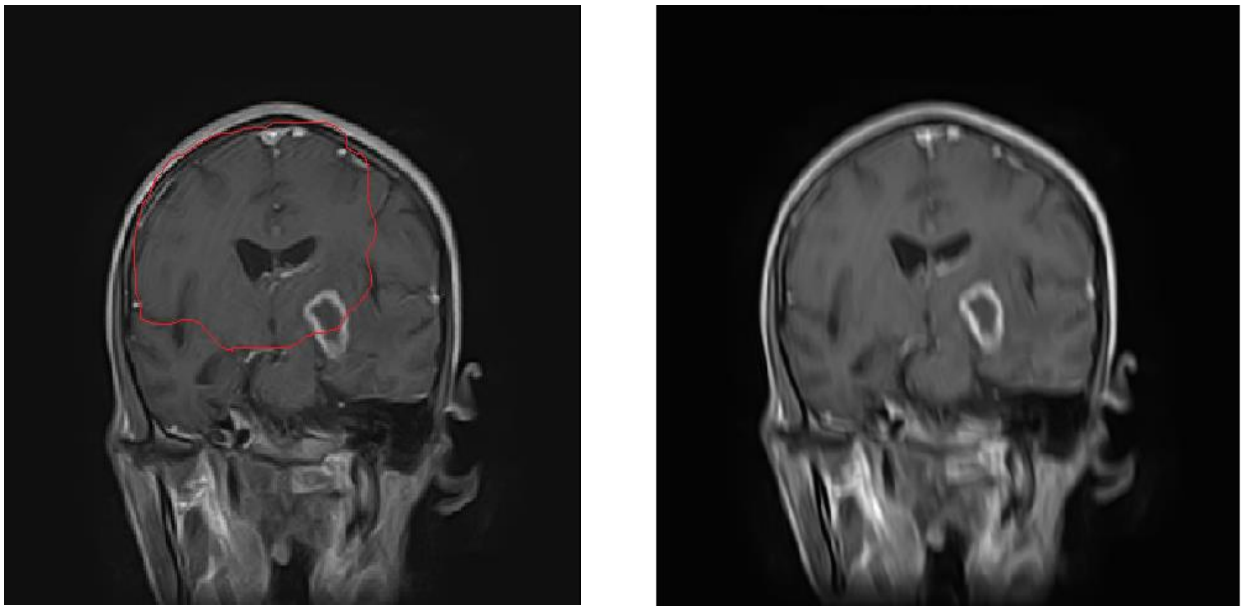

Figure 5.2 Comparison between the original coronal MRI image (L) and the corrected image(R) with angle 99° and length 11.

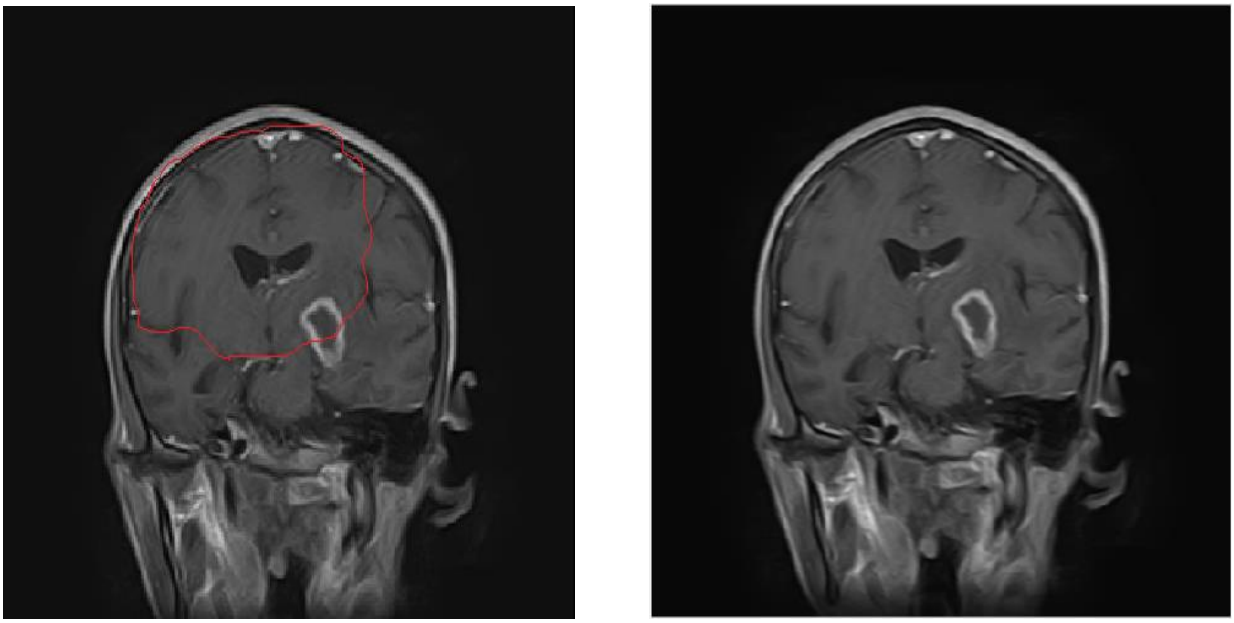

Figure 5.3 Comparison between the original coronal MRI image (L) and the corrected image(R) with angle 173° and length 5.

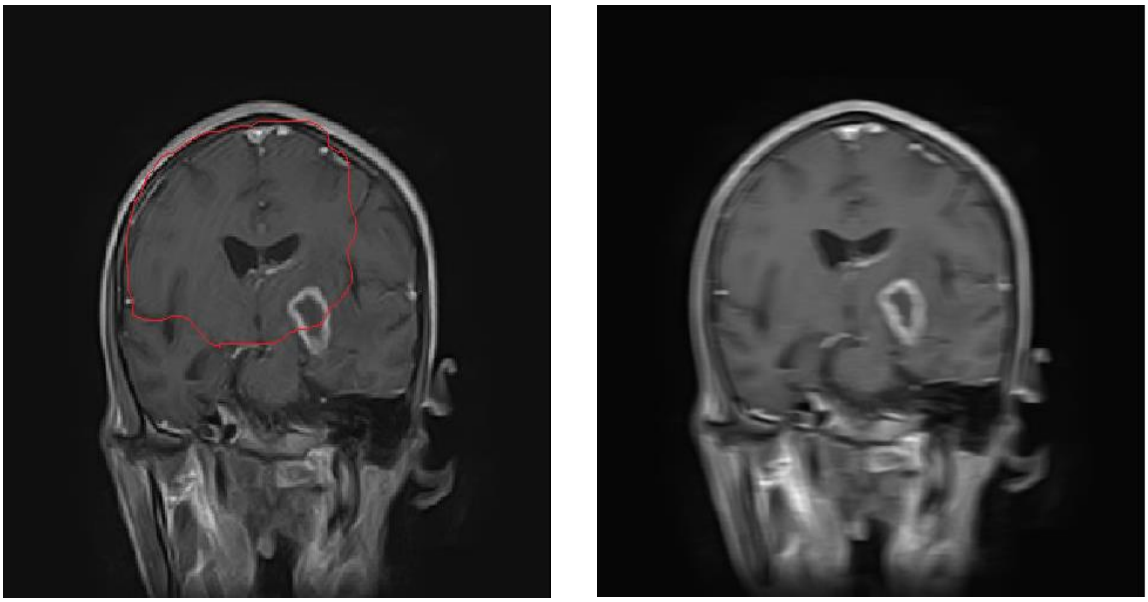

Figure 5.4 Comparison between the original coronal MRI image (L) and the corrected image(R) with angle 179° and length 13.

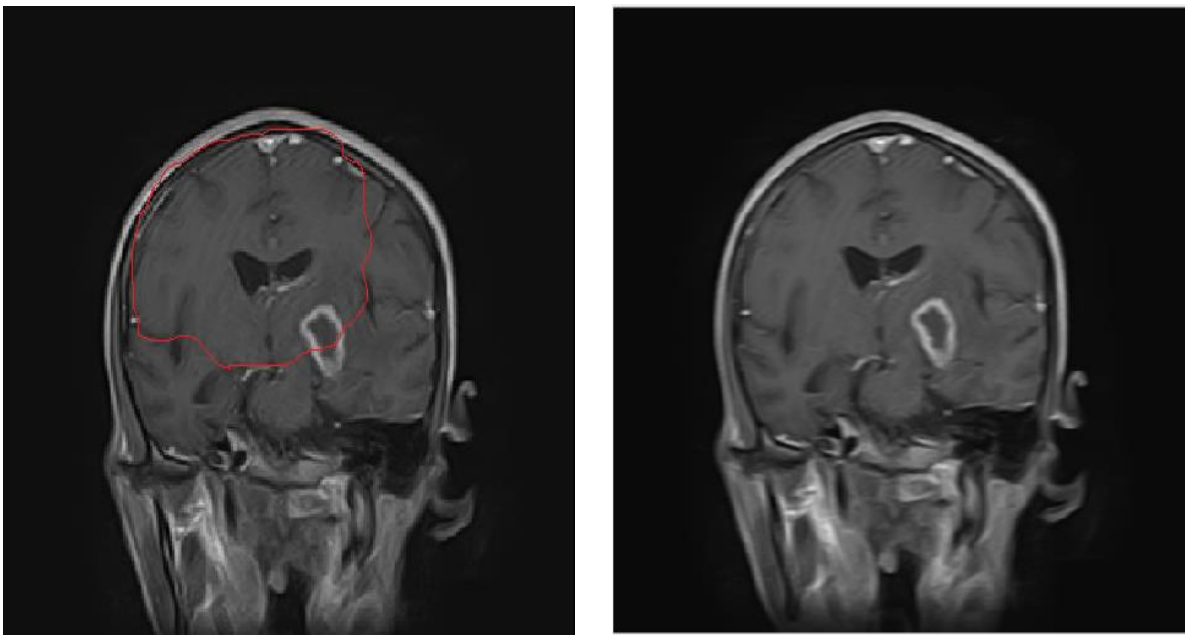

Figure 5.5 Comparison between the original coronal MRI image (L) and the corrected image(R) with angle 2° and length 7.

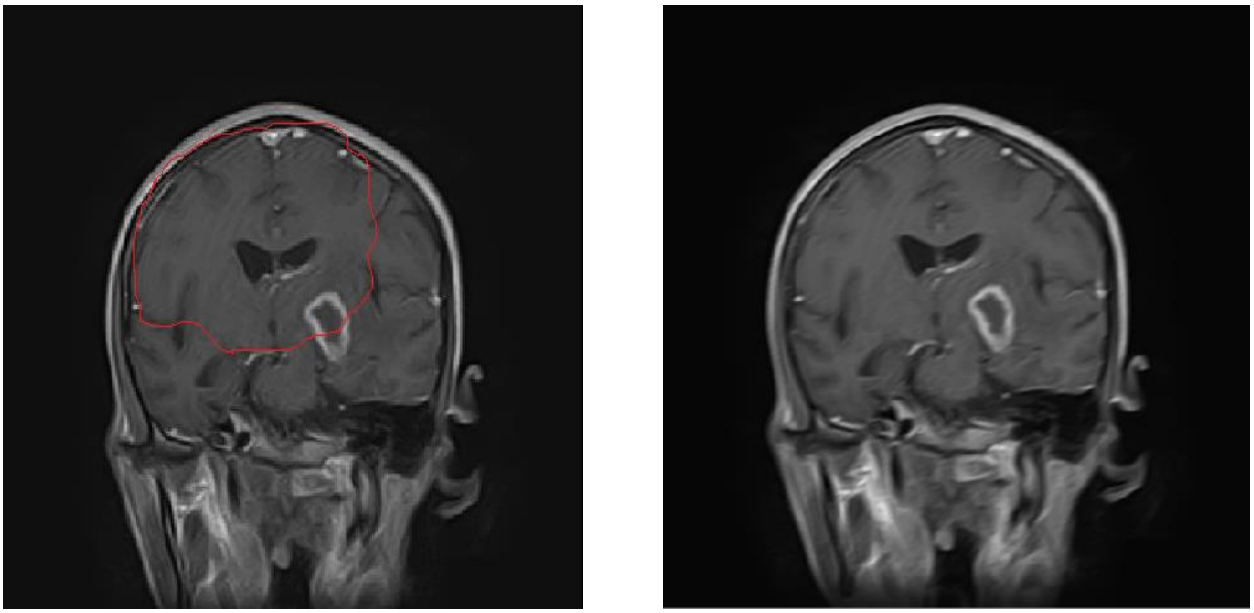

Figure 5.6 Comparison between the original coronal MRI image (L) and the corrected image(R) with angle 16° and length 7.

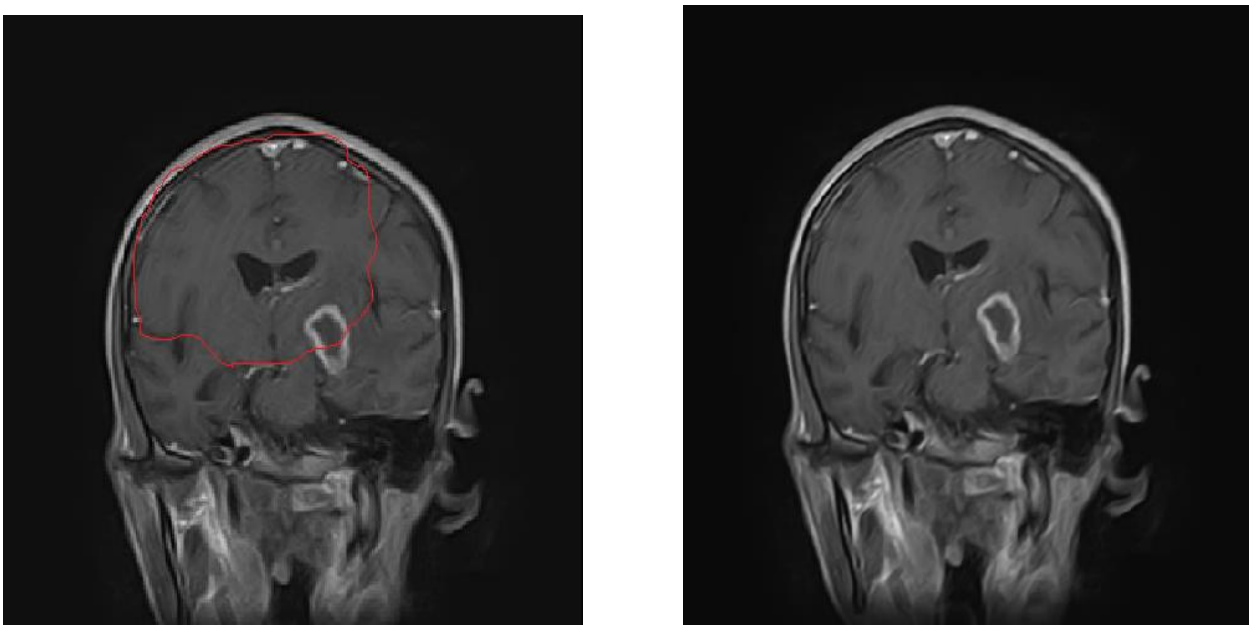

Figure 5.7 Comparison between the original coronal MRI image (L) and the corrected image(R) with angle 62° and length 4.

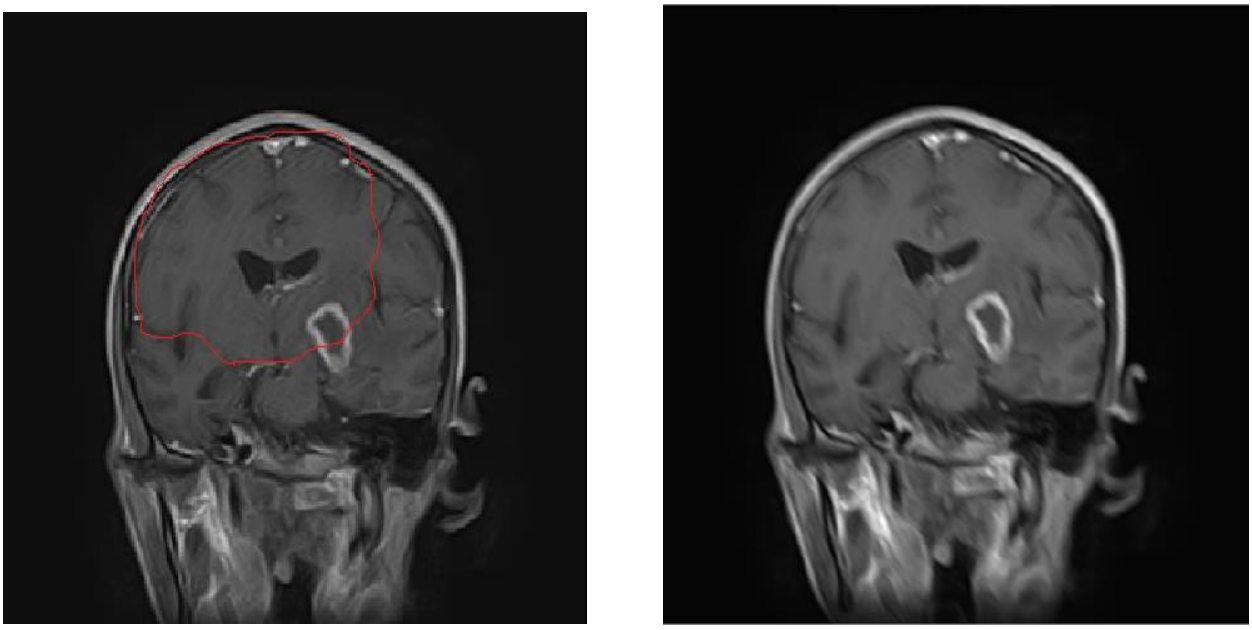

Figure 5.8 Comparison between the original coronal MRI image (L) and the corrected image(R) with angle 131° and length 9.

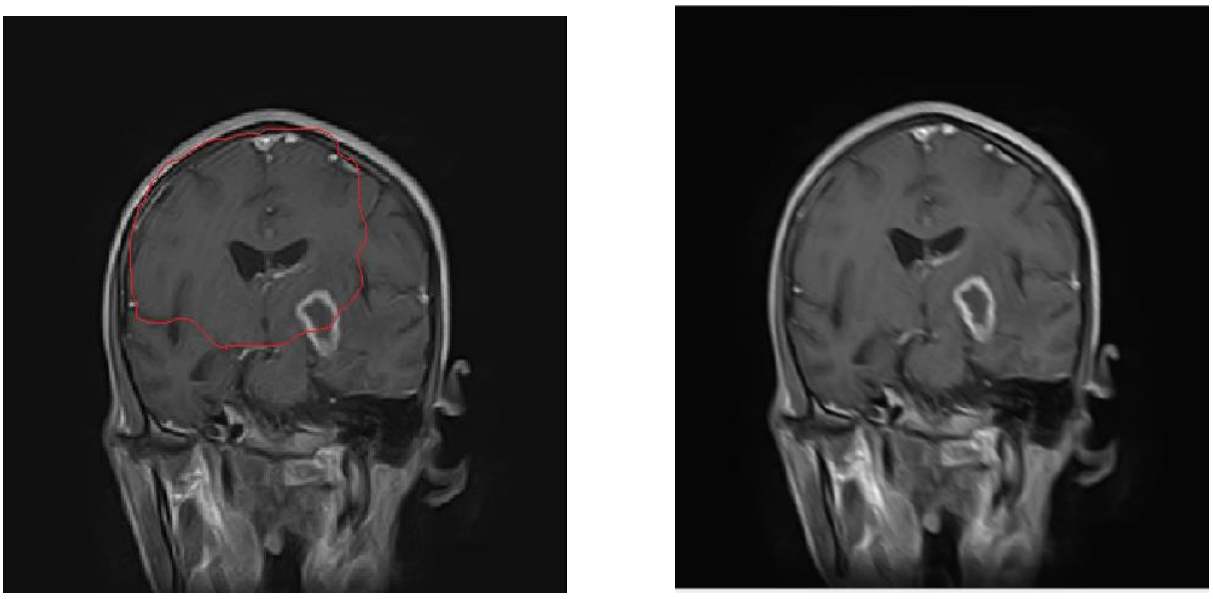

Figure 5.9 Comparison between the original coronal MRI image (L) and the corrected image(R) with angle 145° and length 7.

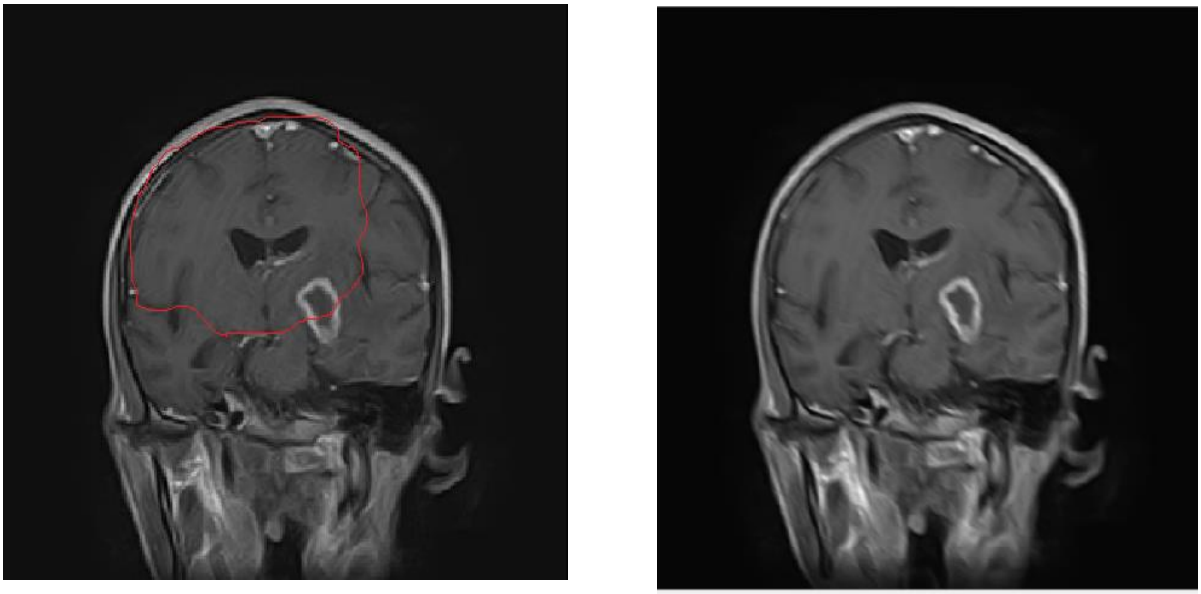

Figure 5.10 Comparison between the original coronal MRI image (L) and the corrected image(R) with angle 124° and length 4.

The following table include the estimated SNR for coronal corrected image in different angles and lengths comparing with the motion blurred image.

Table 5.1 comparison between SNR of motion image and corrected image (coronal image).

Estimated angle &length	**Motion blurred image SNR**	**corrected image SNR**
Figure 5.1, length: 11, angle: 112	-2.4619	-0.81093
Figure 5.2, length: 11, angle: 99	-2.4619	-0.69318
Figure 5.3, length: 5, angle: 173	-2.4619	-2.3216
Figure 5.4, length: 13, angle: 179	-2.4619	-1.4268
Figure 5.5, length: 7, angle: 2	-2.4619	-2.1138
Figure 5.6, length: 7, angle: 16	-2.4619	-1.9739
Figure 5.7, length: 4, angle: 62	-2.4619	-2.1776
Figure 5.8, length: 9, angle: 131	-2.4619	-1.4626
Figure 5.9 length: 7, angle: 145	-2.4619	-1.8852
Figure 5.10 length: 4, angle: 124	-2.4619	-2.2321

By the visual inspection and consultation of radiologist and senior technologist comparing the original motion blurred image and motion corrected image. There is some anatomical structure were going to be diagnosable and clear more than before correction specially in angle 99° fig (5.2) and angle 112° fig (5.1)with the same length 11.

The table above (5.1) contains the ten corrected image with their angles, lengths and SNR. Angle 99° fig (5.2) had the maximum SNR value in the table which determines that it has the better motion blur correction even by the visual inspection the correction was clear and given clear result in the coronal brain MRI image.

Figure 5.3 with angle 173° and length 5 had the minimum SNR value hence lowest degree of motion blur correction.

For the remaining corrected image they gave some degrees of correction but different values of motion distortion was remained in the image and that is why the correction algorithm take different value of expected angles and lengths.

By the visual inspection comparing the original motion blurred image and motion corrected image. There is some anatomical structure was going to be diagnosable and clear more than before correction specially in angle 99° and angle 112° with the same length 11.

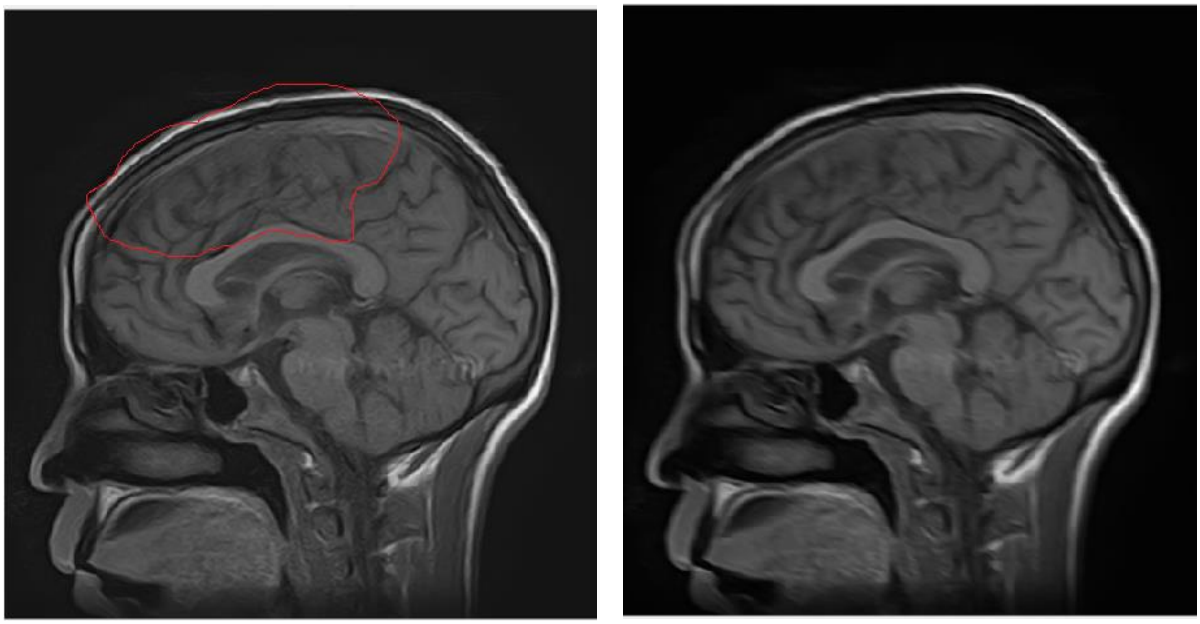

Figure 5.11 Comparison between the original sagittal MRI image (L) and the corrected image(R) with angle 160° and length 8.

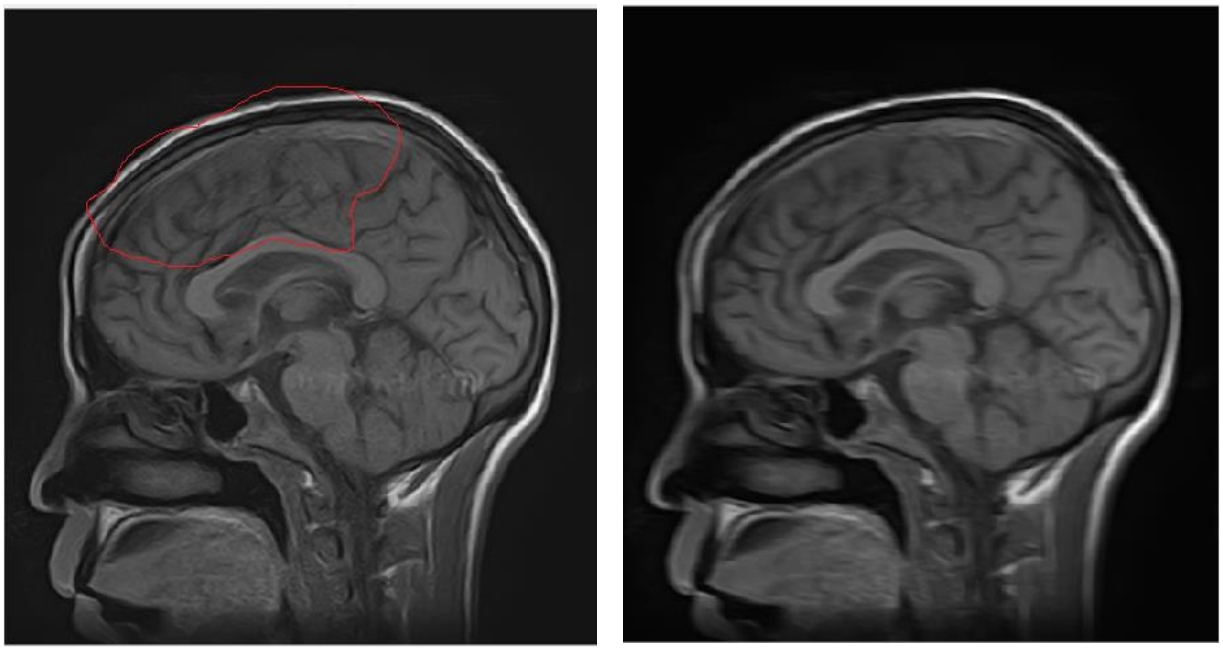

Figure 5.12 Comparison between the original sagittal MRI image (L) and the corrected image(R) with angle 173° and length 9.

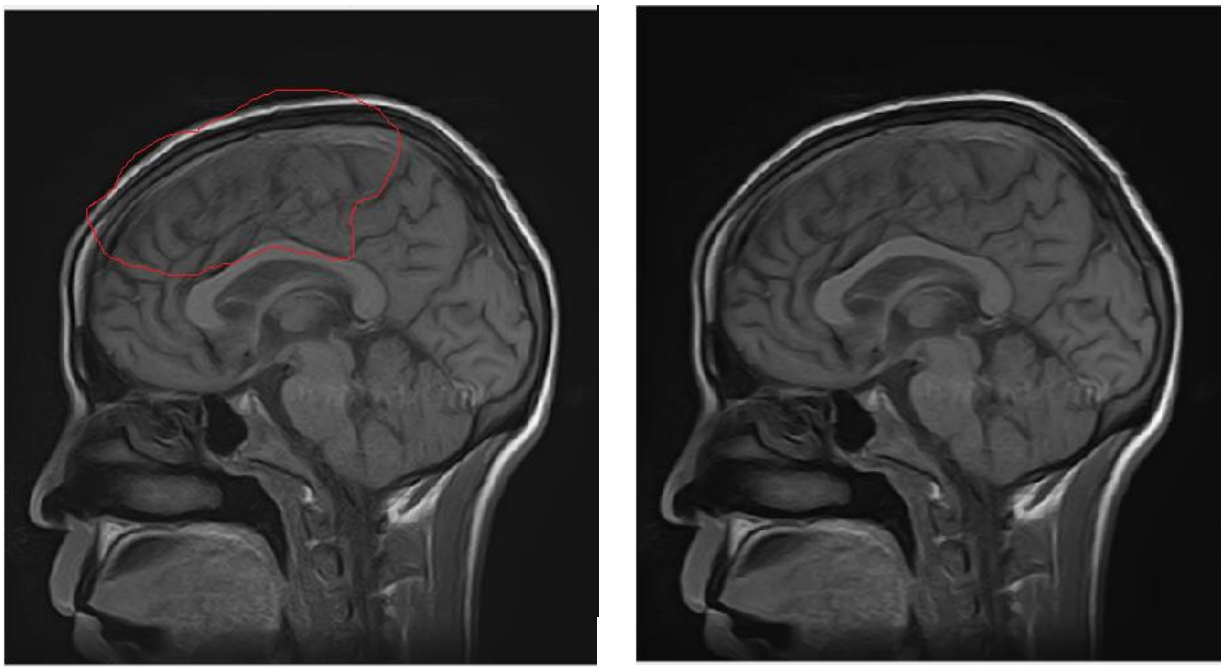

Figure 5.13 Comparison between the original sagittal MRI image (L) and the corrected image(R) with angle 179° and length 4.

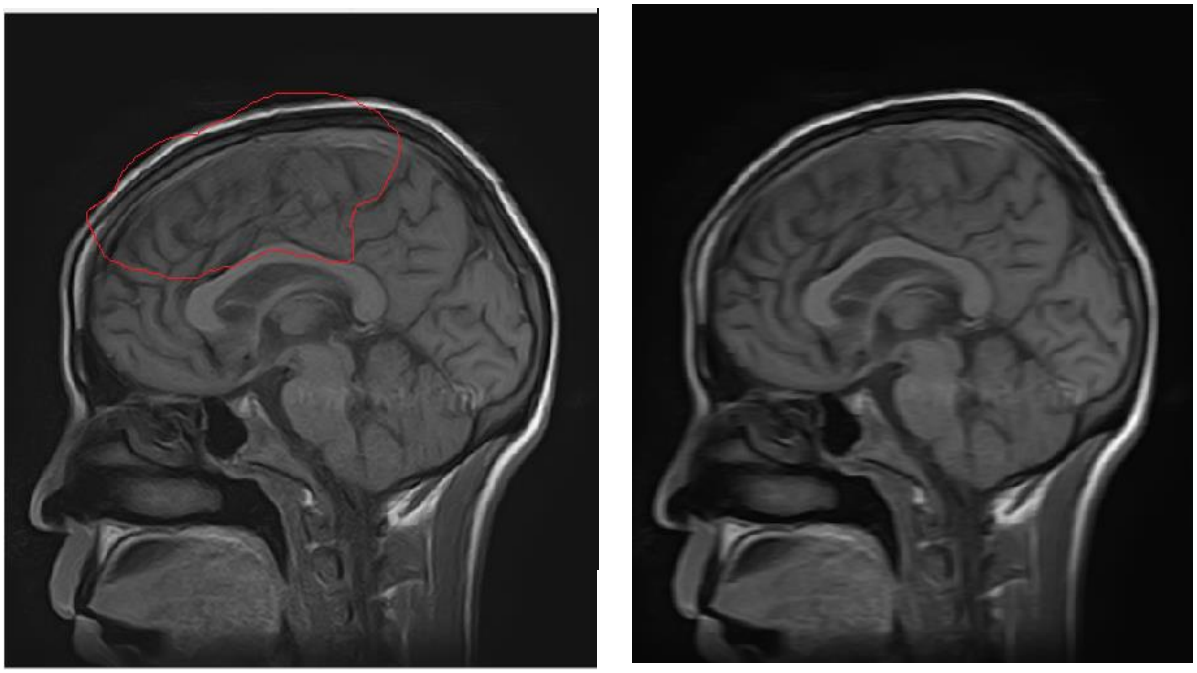

Figure 5.14 Comparison between the original sagittal MRI image (L) and the corrected image(R) with angle 2° and length 8.

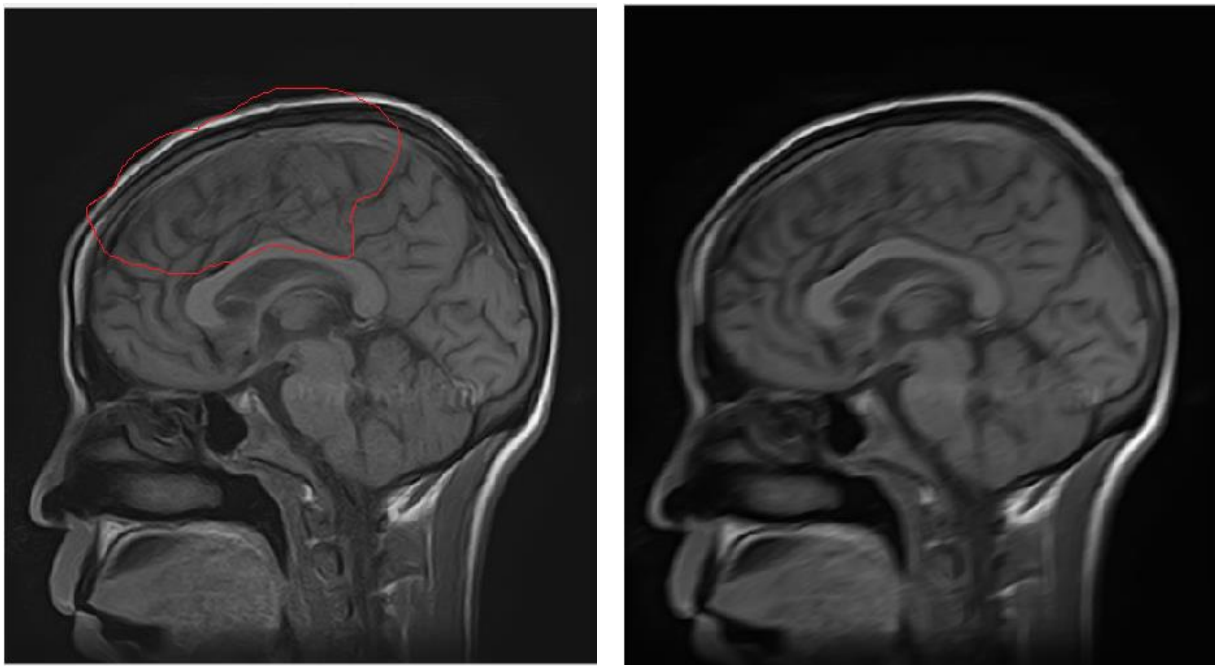

Figure 5.15 Comparison between the original sagittal MRI image (L) and the corrected image(R) with angle 21° and length 11

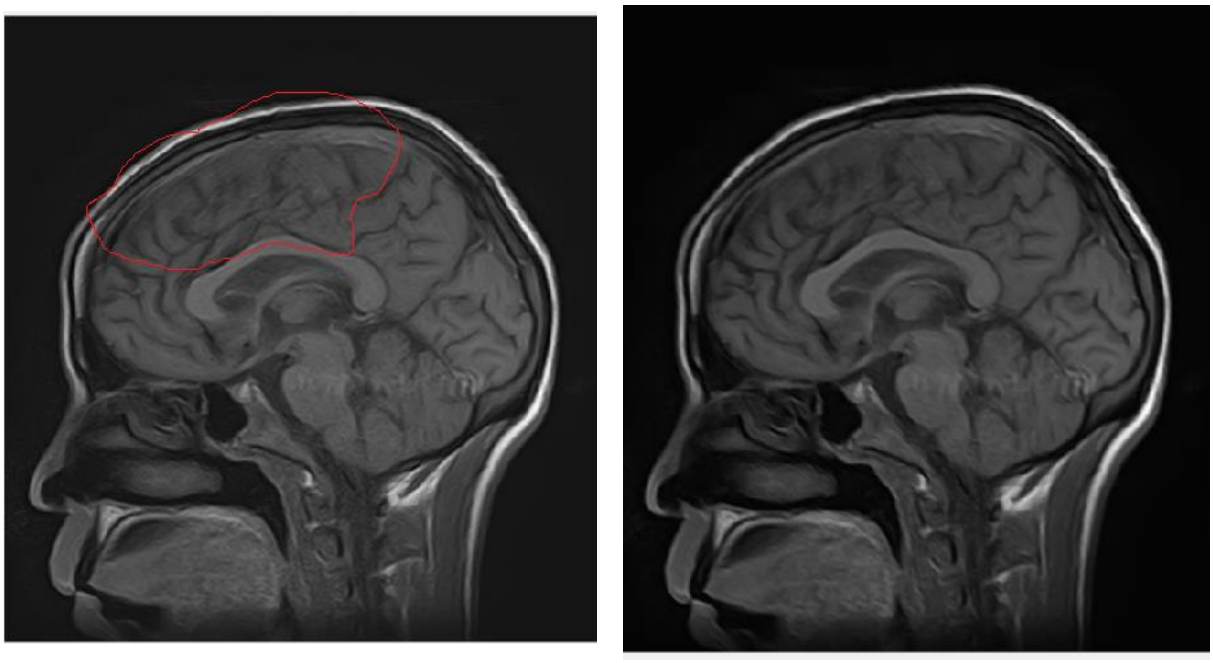

Figure 5.16 Comparison between the original sagittal MRI image (L) and the corrected image(R) with angle 144° and length 4

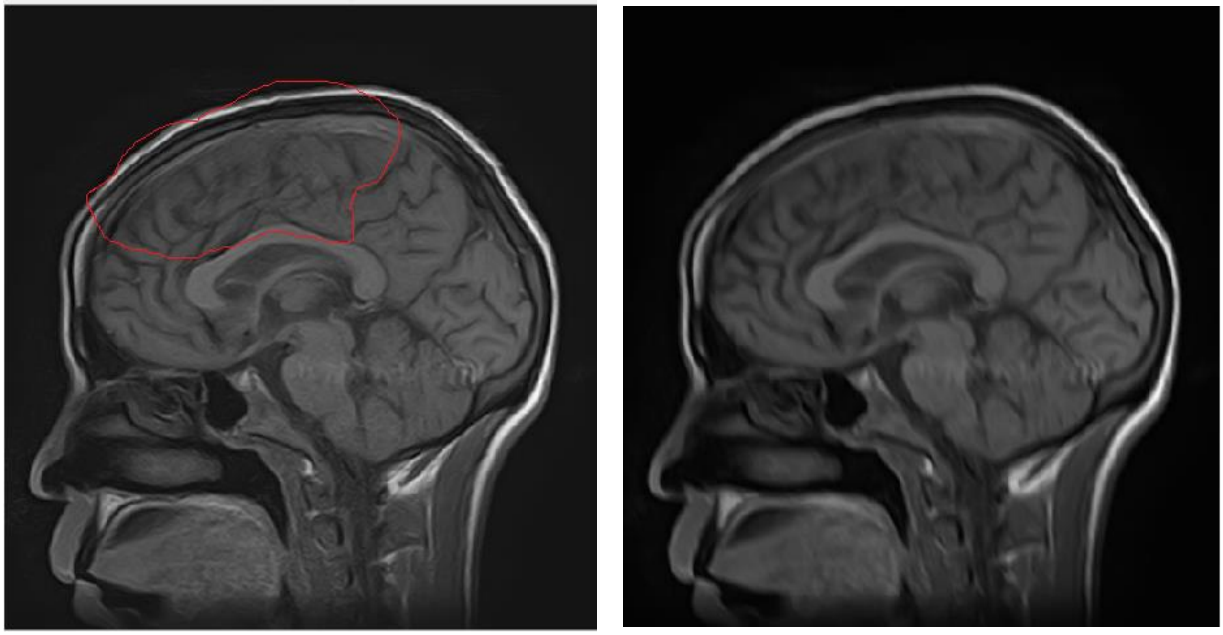

Figure 5.17 Comparison between the original sagittal MRI image (L) and the corrected image(R) with angle 110° and length 8

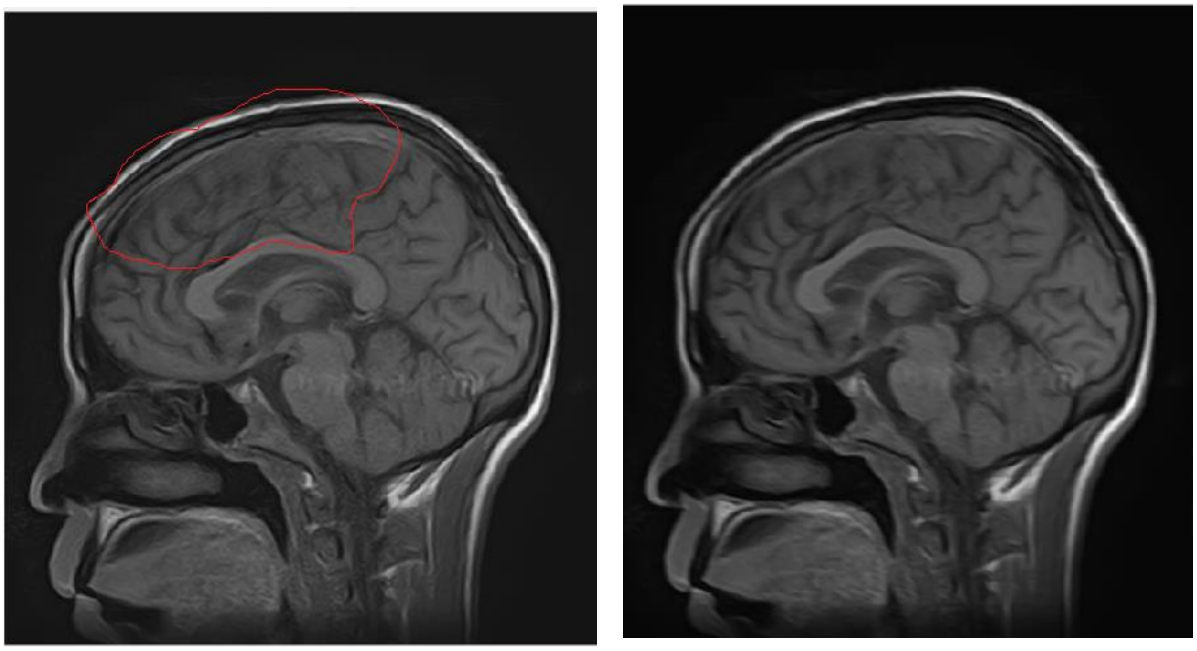

Figure 5.18 Comparison between the original sagittal MRI image (L) and the corrected image(R) with angle 167° and length 6

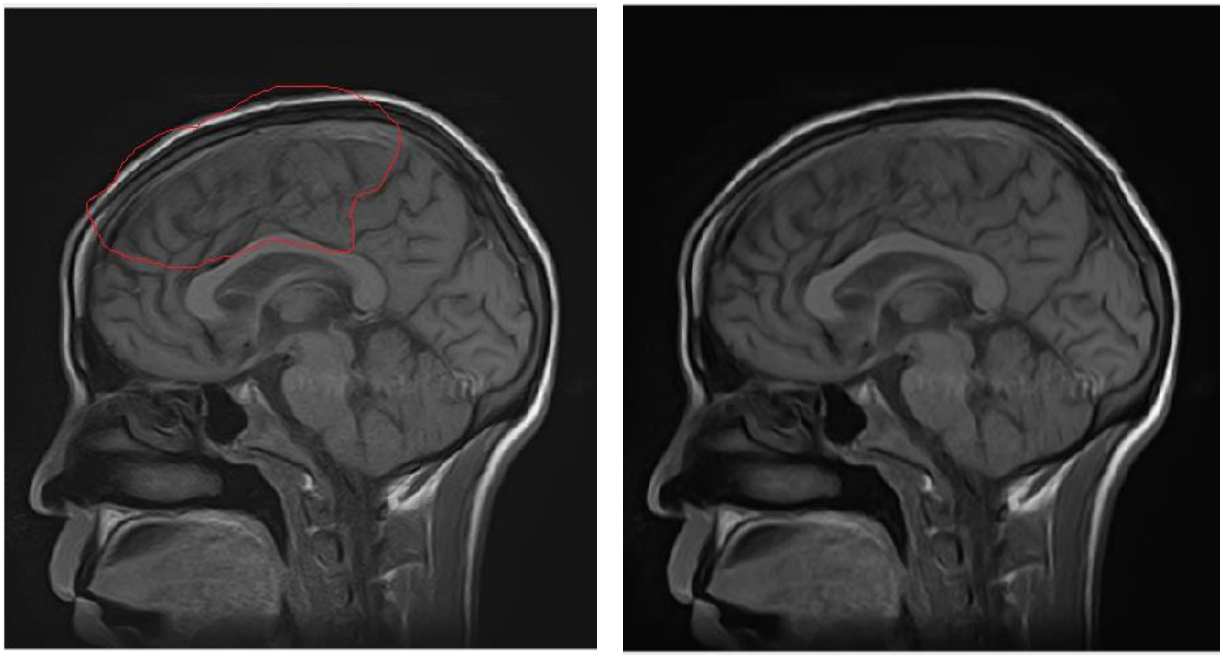

Figure 5.19 Comparison between the original sagittal MRI image (L) and the corrected image(R) with angle 97° and length 4

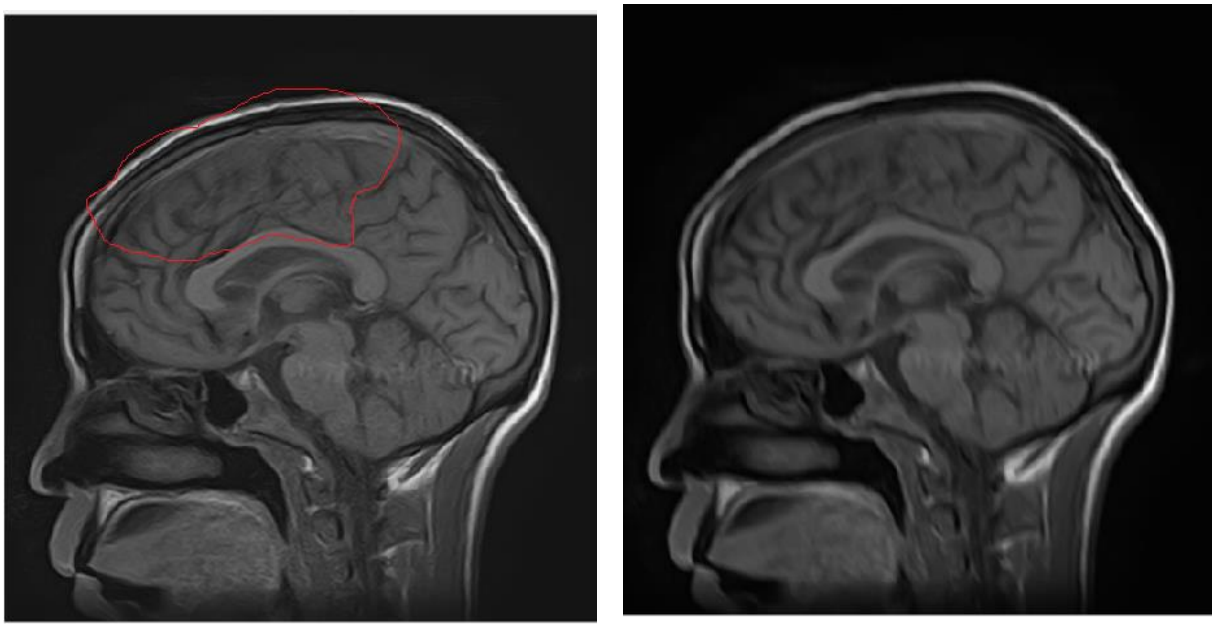

Figure 5.20 Comparison between the original sagittal MRI image (L) and the corrected image(R) with angle 85° and length 4

The following table include the estimated SNR for sagittal corrected image in different angles and lengths comparing with the motion blurred image.

Table 5.2 comparison between SNR of motion image and corrected image (sagittal image) .

Estimated angle &length	**Motion blurred image** SNR	**Corrected image SNR**
Figure 5.11, length: 8, angle: 160	-1.9574	-1.3257
Figure 5.12, length: 9, angle: 173	-1.9574	-1.4007
Figure 5.13, length: 4, angle: 179	-1.9574	-1.9885
Figure 5.14, length: 8, angle: 2	-1.9574	-1.6115
Figure 5.15, length: 11, angle: 21	-1.9574	-0.97155
Figure 5.16, length: 4, angle: 144	-1.9574	-1.7722
Figure 5.17, length: 8, angle: 110	-1.9574	-0.53943
Figure 5.18, length: 6, angle: 167	-1.9574	-1.6416
Figure 5.19 length: 4, angle: 97	-1.9574	-1.4803
Figure 5.20 length: 4, angle: 85	-1.9574	-1.4892

Also in the sagittal image the visual inspection and consultation of radiologist and senior technologist comparing the original motion blurred image and motion corrected image. There is some anatomical structure were going to be diagnosable and clear more than before correction specially in fig(5.12) angle 173°,and fig(5.14)with angle2°, fig(5.15) with angle 21° and fig(5.17) with angle 110° .

The table above (5.2) contain the ten corrected image with their angles, lengths and SNR. Angle 21° fig (5.15) and angle 110° fig (5.17) had the maximum SNR value in the table which determine that it has the better motion blur correction even by the visual inspection the correction was clear and given clear result in the sagittal brain MRI image.

For the remaining corrected image they gave some degrees of correction but different values of motion distortion was remained in the image and that is why the correction algorithm take different value of expected angles and lengths.

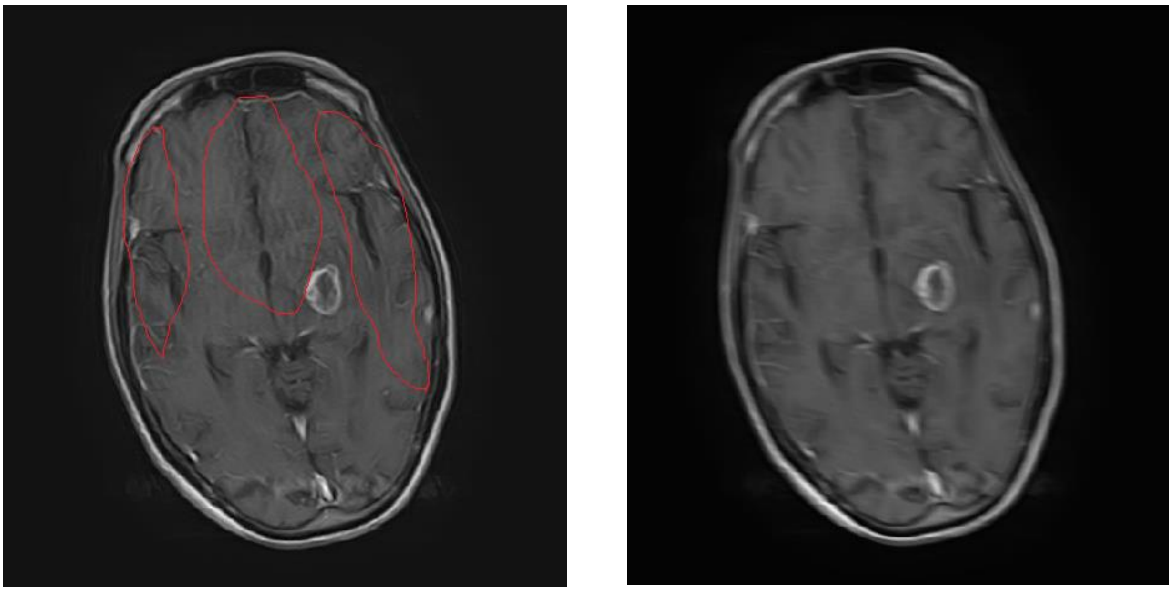

Figure 5.21 Comparison between the original axial MRI image (L) and the corrected image(R) with angle 172° and length 10

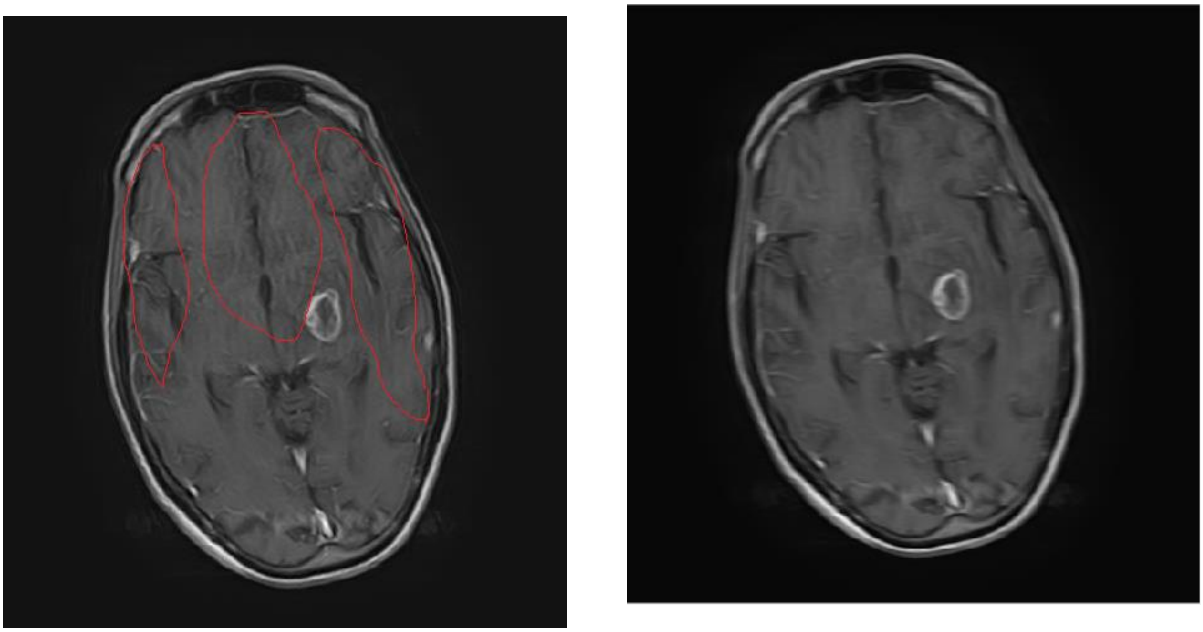

Figure 5.22 Comparison between the original axial MRI image (L) and the corrected image(R) with angle 178° and length 7

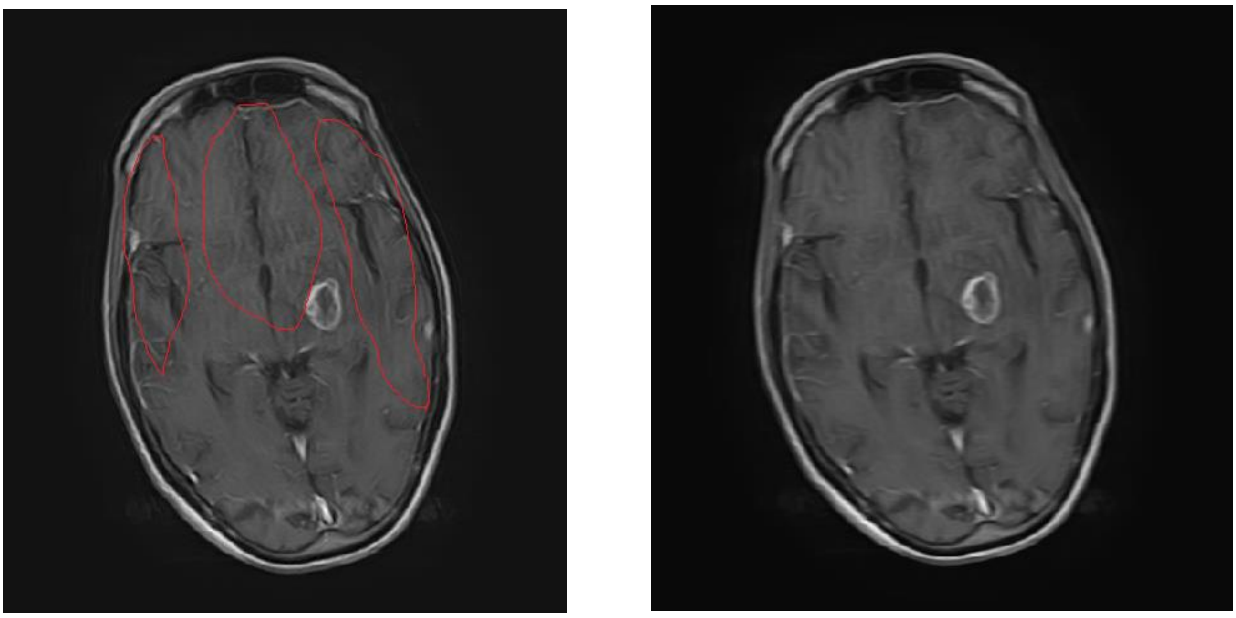

Figure 5.23Comparison between the original axial MRI image (L) and the corrected image(R) with angle 4° and length 6

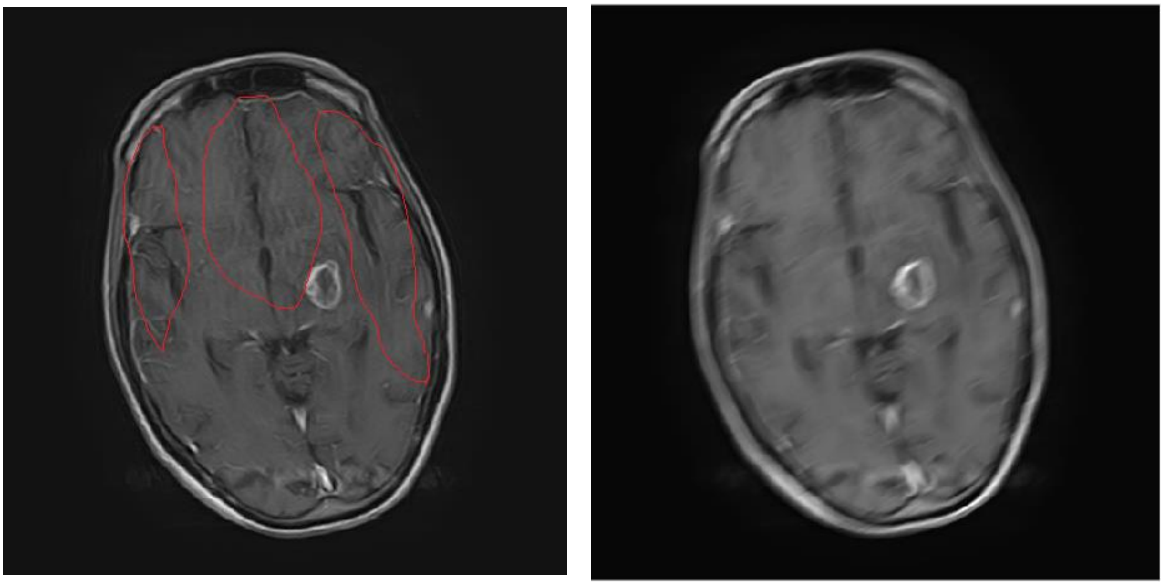

Figure 5.24 Comparison between the original axial MRI image (L) and the corrected image(R) with angle 4° and length 6

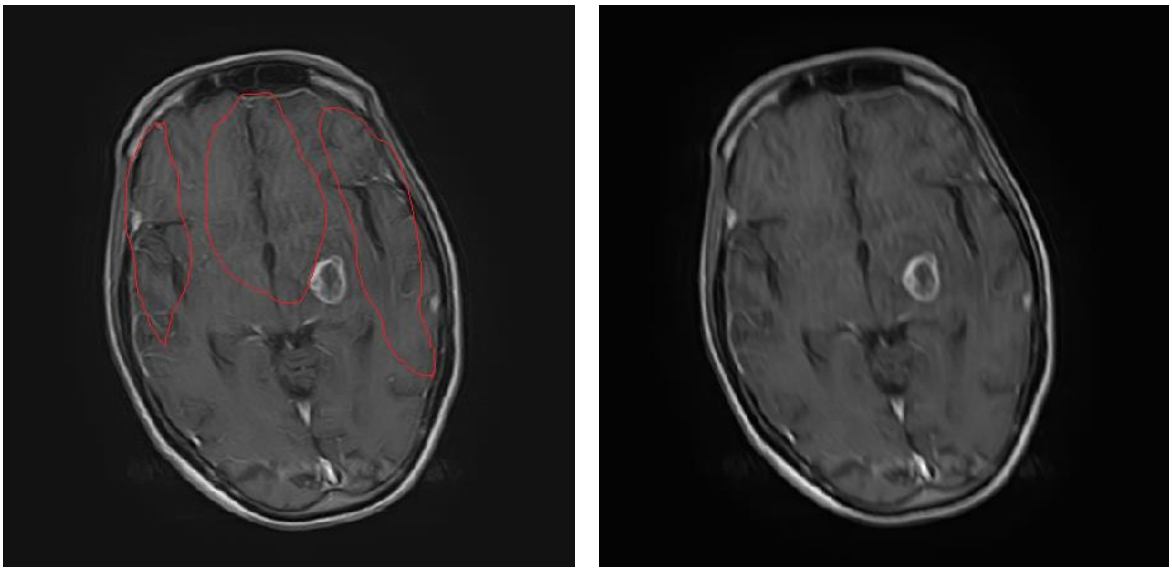

Figure 5.25 Comparison between the original axial MRI image (L) and the corrected image(R) with angle 110° and length 7

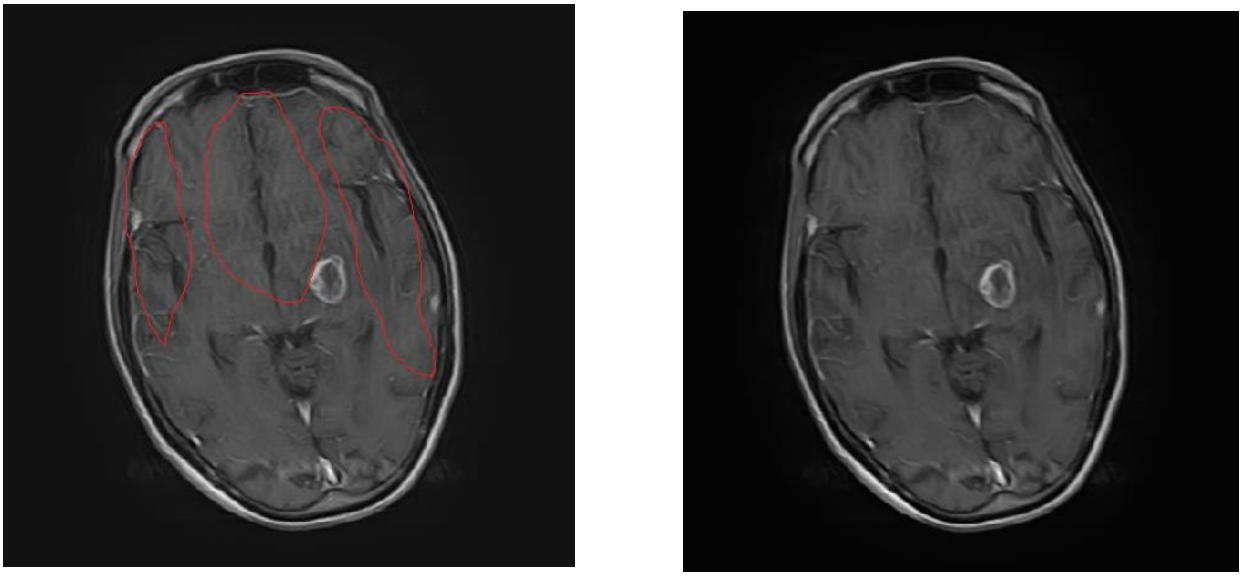

Figure 5.26 Comparison between the original axial MRI image (L) and the corrected image(R) with angle 162° and length 4

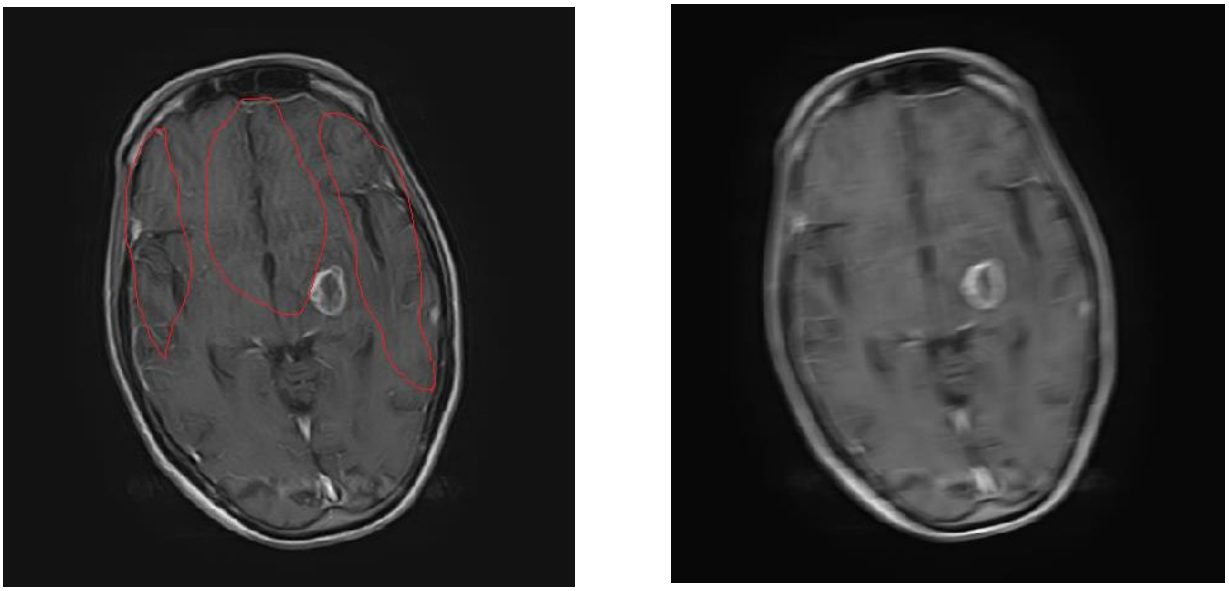

Figure 5.27 Comparison between the original axial MRI image (L) and the corrected image(R) with angle 11° and length 14

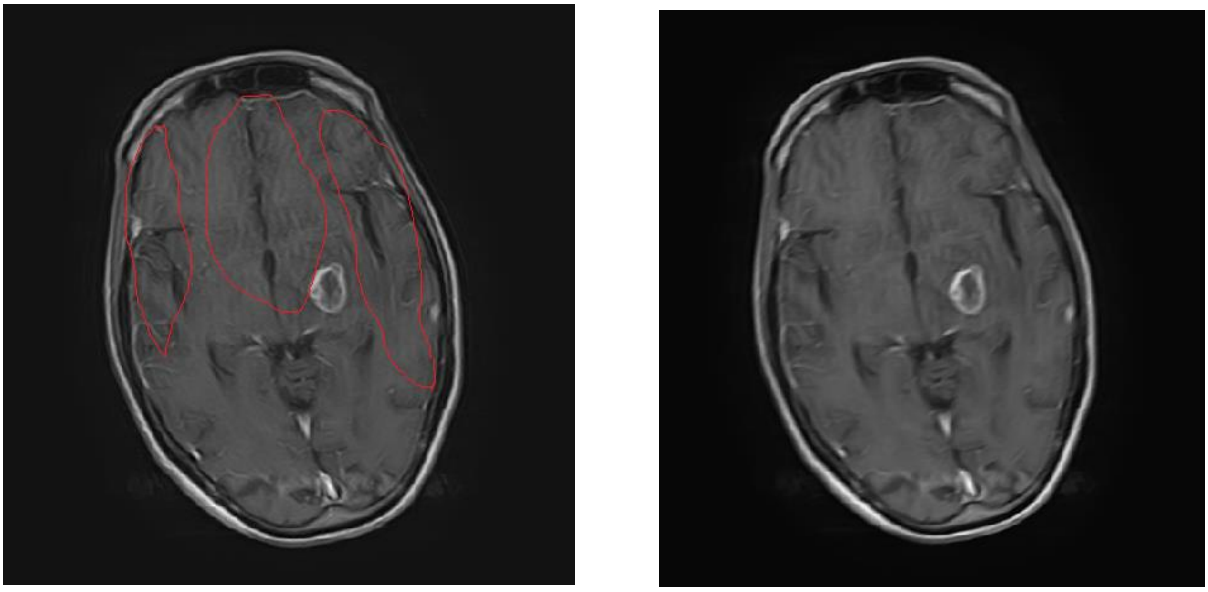

Figure 5.28 Comparison between the original axial MRI image (L) and the corrected image(R) with angle 23° and length 6

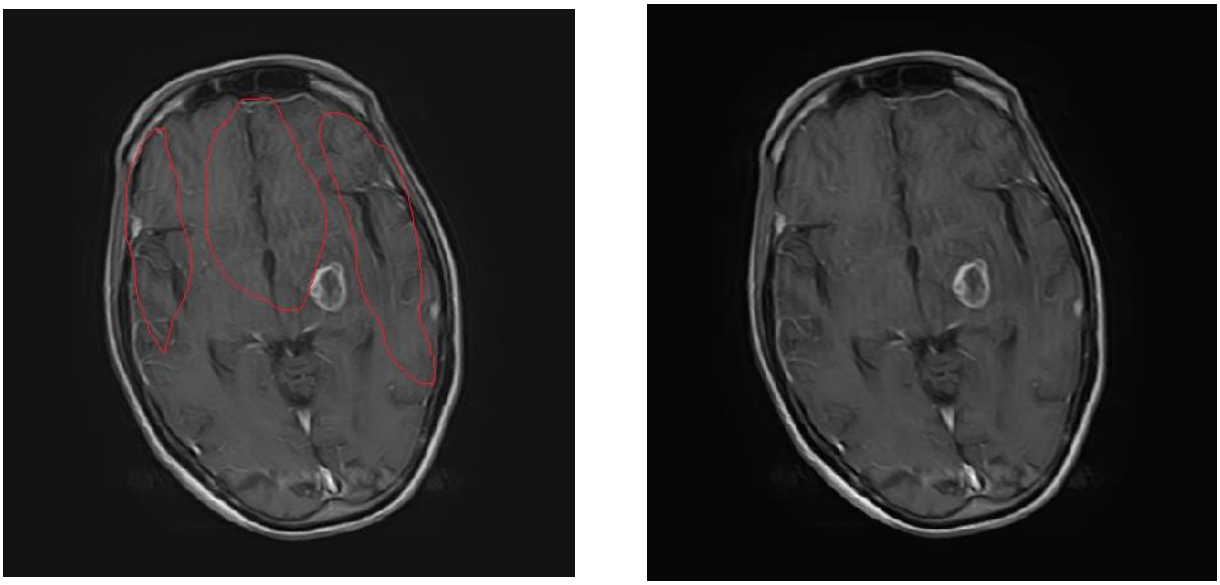

Figure 5.29 Comparison between the original axial MRI image (L) and the corrected image(R) with angle 145° and length 3

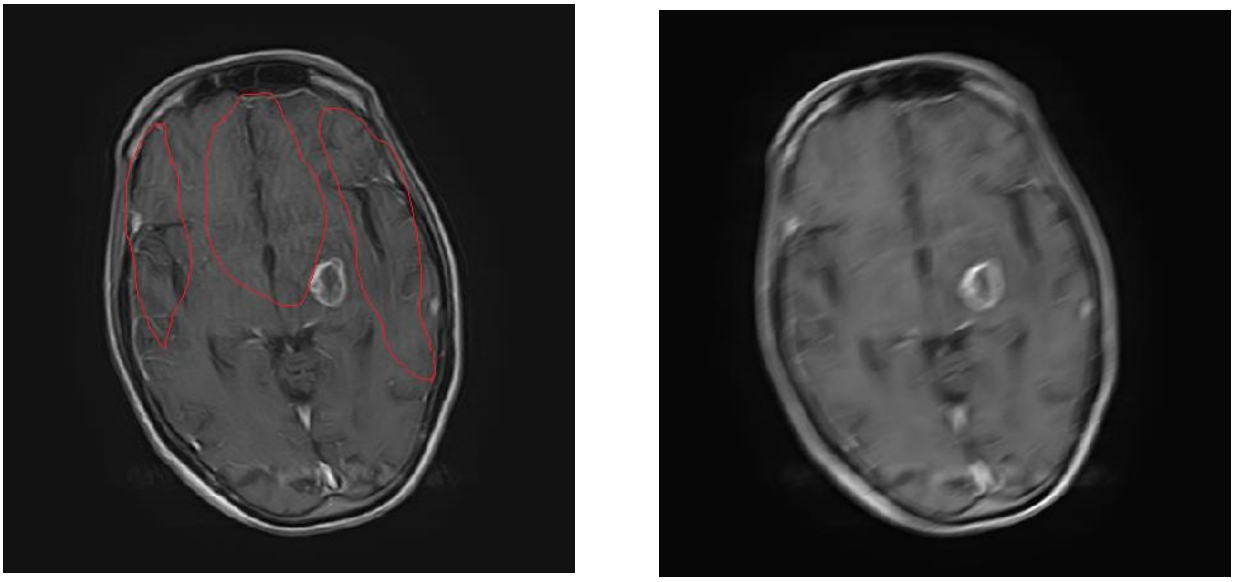

Figure 5.30 Comparison between the original axial MRI image (L) and the corrected image(R) with angle 116° and length 7

The following table include the estimated SNR for sagittal corrected image in different angles and lengths comparing with the motion blurred image.

Table 5.3 comparison between SNR of motion image and corrected image (axial image).

Estimated angle &length	**Motion blurred image SNR**	**corrected image SNR**
Figure 5.21, length: 10, angle: 172	-1.9394	-1.042
Figure 5.22, length: 7, angle: 178	-1.9394	-1.5781
Figure 5.23, length: 6, angle: 4	-1.9394	-1.6497
Figure 5.24, length: 14, angle: 30	-1.9394	0.79873
Figure 5.25, length: 7, angle: 110	-1.9394	-0.62628
Figure 5.26, length: 4, angle: 162	-1.9394	-1.8385
Figure 5.27, length: 14, angle: 11	-1.9394	-0.2526
Figure 5.28, length: 6, angle: 23	-1.9394	-1.3499
Figure 5.29 length: 3, angle: 145	-1.9394	-1.9133
Figure 5.30 length: 7, angle: 116	-1.9394	-0.64491

Finally in the axial corrupted image also by visual inspection and consultation of radiologist and senior technologist comparing the original motion blurred image and motion corrected image. There is some anatomical structure were going to be diagnosable and clear more than before correction specially in fig(5.21) angle 172°,and fig(5.22)with angle 178°, fig(5.15).

The table above (5.3) contain the ten corrected image with their angles, lengths and SNR. Although fig (5.21) angle 172°, and fig (5.22) with angle 178°, fig(5.15).
Had not the maximum SNR value in the table, they had the better motion blur correction even by the visual inspection the correction was clear and given clear result in the axial brain MRI image.

For the remaining corrected image they gave some degrees of correction but different values of motion distortion was remained in the image and that is why the correction algorithm take different value of expected angles and lengths.

CHAPTER Six

6. CONCLUSION AND RECOMMENDATIONS

6.1 Conclusion

In this study, a motion blur correction algorithm, used to assess coronal, sagittal and axial image for the MRI brain corrupted with rigid motion.

Wiener filter was taken as the main algorithm in the correction procedure. According to ten different angles and lengths estimated before starting the correcting procedure.

The correction algorithm achieved the best results which lead to clear appearance in anatomical brain feature and remove the motion blur which can obscure very important details.

Although the corrected image by wiener filter gave a best result, it suffering some degree of unsharpeness, application of sharpening filter was needed and it gave better results.

Motion blur in sagittal image result in highly degree of correction by the algorithm in the research. Since more than five images according to the different degree of angle and length estimation was totally corrected.

6.2 Recommendations and Future Work

Following the algorithm described in this thesis and the other methods of MRI image motion correction in the literature review chapter three indicate that the problem was still remain this is as general.

For developing the results in this research:-

1. Develop more different algorithm.
2. Use different method for sharpening following the corrected image by wiener filter (this is can improve the final result).
3. Using more than ten motion blur angle and length to increase the probability of achieving the maximum motion blur correction.

REFERENCES

[1] Google Internet, “General views”, Copy right J.P-Horn.

[2] Liang Z-P, Lauterbur PC,” Principles of magnetic resonance imaging: a signal processing perspective”, New York, Vol.4, No.16, 2000.

[3] Mohamed Abdullah, A., “the working principle of MRI lecture/Class”, University of medical science and technology, Vol.3, NO.6, 2008.

[4] Rskhandpur, “Hand book of bio medical instrumentation”, second edition, http://books.google.com/books.

[5]Wikipedia, “Hardware of MRI”, http://en.wikipedia.org/wiki/mri.

[6] Perry sprawls, Jr, Ph.D., FACR, “Physical principles of medical Imaging”,

printed in United State of America, Vol.54, No.5, 2008.

[7] Mohamed Abdullah, A, “Hardware of MRI”, University of medical science and technology, Vol.12, No.3, 2008.

[8] Perry sprawls, Ph.D., FACR, FAAPM, “Magnetic resonance imaging”, Department of radiology mory university, Vol.23, No.7, 2009.

[9] Mohamed Abdullah, A, “Artifact of MRI”, University of medical science and technology, Vol.55, No.11, 2008.

[10] Atkinson D,” Magnetic Resonance Imaging II”, Magnetic Resonance in Medicine, Vol.44, No.9, 2012.

[11] Matthias Schlogl,” Motion Correction in MRI”, Magnetic Resonance in Medicine, Vol.13, NO.5, 2013.

[12] Mark Jenkinson, Peter Bannister, “Improved Optimization for the Robust and Accurate Linear Registration and Motion Correction of Brain Images”, Elsevier Science (USA), Vol.17, No.10, 2002.

[13]Stefan Thesen, Oliver Heid,” Prospective Acquisition Correction for Head Motion with Image-based Tracking for Real-Time fMRI”, Computer methods in Biomechanics and Biomedical engineering,Vol.30,No.11,2009.

[14] Timothy T. Brown, Joshua M. Kuperman,” Prospective motion correction of high-resolution magnetic resonance imaging data in children”, journal homepage: www.elsevier.com/locate/ynimg,Vol.53,No.2,2010.

[15] Gary H. Glover, Tie-Qiang Li, “Image-Based Method for Retrospective Correction of Physiological Motion Effects in fMRI: RETROICOR”, Magnetic Resonance in Medicine, Vol.44, No.8, 2000.

[16] Peter Kochunov, Jack L. Lancaster, “Retrospective Motion Correction Protocol for High-Resolution Anatomical MRI”, Human Brain Mapping, Vol.27, No.11, 2006.

[17] Alexander Loktyushin, Hannes Nickisch, “Blind Retrospective Motion Correction of MR Images”, Medical Imaging, Vol.55, No.7, 2007.

[18] James G. Pipe, “Periodically Rotated Overlapping ParallEL Lines with Enhanced Reconstruction (PROPELLER) MRI; Application to Motion Correction”, Proceedings of the International Society for Magnetic Resonance in Medicine Sixth Scientific Meeting and Exhibition Sydney, V0l.22, NO.5, 2011.

[19] Belma Dogdas, Quanzheng Li, “Motion Correction with Propeller MRI: Application to Head Motion”, International Journal of Electrical, Electronics and Computer Systems, Vol.26, No.12, 2010.

[20] Julian Maclaren, Michael Herbst, "Prospective Motion Correction in Brain Imaging: A Review", Suffix Indicating a Corporation, Vol.23, No.6, 2012.

[21] Shamik Tiwari, V. P. Shukla," Review of Motion Blur Estimation Techniques", *Image and Graphics,Vol.1,No.4,2013.*

[22] R. C. Gonzalez and R. E. Woods, "*Digital Image Processing"*, Prentice Hall, Vol.33, No.4, 2007.

[23] MATLAB tool books, www.mathwork.com.